Li Bao*, Jia Ma, Weimin Long, Peng He, Ting-an Zhang and Anh V. Nguyen

Fractal analysis in particle dissolution: a review

Abstract: Fractal is a geometric language to describe the objects, the systems, and the phenomenon spatially and temporally. This paper reviews the literature on fractal models developed to describe the dissolution of particles. Dissolution, the process by which a solid forms a homogeneous mixture with a solution, is the behavior of a population of particles rather than a single one in most of the cases. The fractal models developed for the particle population are reviewed on the basis of two key particle surface properties, namely, the surface fractal nature and the chemical reactivity of particle surfaces. In terms of the surface fractal nature, fractals have been used to describe the change in the superficial roughness of particles, surface area-particle size relation, and particle size distribution (PSD). In terms of the reactive fractal dimensions, the models that describe the dissolution process have been developed to obtain the empirical noninteger exponent, the reactive fractal dimension that can dictate the chemical reactivity of a solid surface. The comparison between the surface fractal dimension and the reactive fractal dimension provides the dissolution mechanisms in many aspects of surface morphology. Further research is necessary to modify the current models to coincide with the real industrial processes and production and to develop the specific models for a better understanding of many processes involving the dissolution of particles encountered in many areas, including pharmaceutical and chemical applications and hydrometallurgy.

Keywords: dissolution; fractal dimension; fractals; particle size; reaction rate; surface area.

DOI 10.1515/revce-2013-0032
Received October 7, 2013; accepted March 20, 2014; previously published online May 15, 2014

***Corresponding author: Li Bao,** State Key Laboratory of Advanced Brazing Filler Metals and Technology, Zhengzhou Research Institute of Mechanical Engineering, Zhengzhou 450001, China, e-mail: baoli-1983@163.com
Jia Ma and Weimin Long: State Key Laboratory of Advanced Brazing Filler Metals and Technology, Zhengzhou Research Institute of Mechanical Engineering, Zhengzhou 450001, China
Peng He: State Key Laboratory of Advanced Welding and Joining, Harbin Institute of Technology, Harbin 150001, China
Ting-an Zhang: School of Materials and Metallurgy, University of Northeastern University, Shenyang 110819, China
Anh V. Nguyen: School of Chemical Engineering, The University of Queensland, Brisbane, Queensland 4072, Australia

1 Introduction

Dissolution is the process by which a solid or liquid forms a solution in a solvent. In solids, this can be explained as the breakdown of the crystal lattice into individual ions, atoms, or molecules and their transport into the solvent. The heterogeneous process occurs on the boundary between two phases, which is called the phase interface. Dissolution testing is widely used in the pharmaceutical and hydrometallurgical industries for the optimization of formulation and quality control.

There are two types of reactions on the interface that might impact the particle size and the reaction kinetics. The first case is that the resultant is able to dissolve in the solution, that is, no insoluble product appears. The pharmaceutical and crystalline solid compound dissolution into the aqueous solution belongs to this type, which is expressed as (Hua 2004)

$$a\mathrm{A(s)}=b\mathrm{B(aq)}+c\mathrm{C(aq)} \quad (1)$$

as well as some of the metallurgical leaching processes such as the leaching copper oxide in acid and digesting gibbsite into sodium aluminate solution (Leeson and Carstensen 1974, Hua 2004):

$$a\mathrm{A(s)}+b\mathrm{B(aq)}=c\mathrm{C(aq)}+d\mathrm{D(aq)}. \quad (2)$$

In this case, the heterogeneous reaction on the solid surface can be divided into the following steps: (i) diffusion of the interacting substances to the surface, (ii) adsorption on the surface, (iii) reaction on the surface, (iv) desorption from the surface, and (v) diffusion of the products from the surface (Hua 2004). The total reaction rate of the heterogeneous reaction depends on the step that is the slowest. Since the adsorption and desorption are usually much faster than the reaction, the dissolution kinetics will be limited either by molecular diffusion (diffusion limited or mass transfer limited) or by the surface reaction (reaction limited).

The diffusion transports the dissolved substance across a diffusion layer where the concentration of the dissolved substance continuously decreased from the concentration of the saturated solution at the solid surface (C_s) to the concentration level (C) in the bulk solution. According to the first Fick's law, the rate of diffusion is formulated as (Hua 2004)

$$-\frac{dN}{dt}=\eta S(C_s-C) \tag{3}$$

where N is the amount of the dissolved substance within time interval t, η is the diffusion coefficient in the liquid phase, and S is the total surface of the dissolved solid substance.

In this case, the thickness of the boundary layer depends on the fluid dynamics. In other words, the stirring strength affects the reaction rate remarkably. The reaction rate is proportional to the concentration of the liquid reactant. The dissolving temperature hardly impacts the rate.

When the dissolving process is controlled by the reaction, the dissolving rate depends on the temperature, and the stirring strength does not work on the rate. The dissolution rate is the rate of reaction (Hua 2004):

$$-\frac{dN}{dt}=\xi SC_s^n. \tag{4}$$

Here, ξ is the reaction constant on the interface and n is the reaction order.

On the contrary, if the product cannot dissolve into the aqueous solution, the general expression of this case is (Hua 2004)

$$a\mathrm{A(s)}+b\mathrm{B(aq)}=c\mathrm{C(s)}+d\mathrm{D(aq)}. \tag{5}$$

In the context, a layer that could not react with the solute forms outside the unreacted part of a particle. This layer, called the ash layer, might resist the solute moving from the bulk solution to the reacting interface (Levenspiel 1972). Thus, with the exception of the five reaction steps above, one should not neglect the influence of the ash layer on the diffusion of the solute to the surface of the unreacted solid and/or soluble to the solution. If the diffusion through the ash layer is the slowest step, the dissolution kinetics is ash-layer diffusion limited. The dissolution rate is mainly affected by the concentration of reactant, the stirring strength, and the dissolving temperature. The dissolution rate is expressed as (Hua 2004)

$$-\frac{dN}{dt}=\psi A(C_s-C_s') \tag{6}$$

where ψ is the diffusion coefficient in ash layer, A is the surface area of the unreacted core, and C_s' is the concentration on the interface between the ash layer and the unreacted core. With respect to the reaction-limited dissolution kinetics, the reactive surface area in Equation (4) should be related to the area of the unreacted core A instead of S.

From the dissolution rate equations, one would obviously get that the area of interface and the concentration of dissolved substance on the interface play an important role on the dissolution kinetics. On a molecular level, the reaction-limited reactions correspond to the processes where the activation barrier is much higher than the average energy, while, for the diffusion-limited phenomena, almost every collision of a reactive molecule on the interface leads to a reaction (Mortimer and Taylor 2002). In the former case, if the superficial reactivity is homogeneous on the particle, the concentration of the reactive molecules is constant at any site, resulting in the uniform reactivity at any points on the surface. However, in practice, the mineral particles have such complex compositions that the concentration of the dissolved substance cannot distribute uniformly on the surface, resulting in the uneven superficial reactivity. When the dissolution is controlled by diffusion, for the particle with rough surface in most practical cases, one could expect that the reactivity will locate differently from site to site on the surface whether we consider a hole in the solid or a prominence. Each of these steps, diffusion and reaction, may predominate at different places in the same system. In this instance, the classic kinetic models for describing the dissolution process, such as the progressive conversion model and the unreacted core model, seem to be not applicable. One has to find a new approach to express such imperfect process in the term of industrial practice.

The concept of fractal proposed by Mandelbrot in 1975 (Mandelbrot 1983) for the chaos system is what we need. Starting with the question of how long the coast of Britain is, the amazing fractals have been applied widely in almost every part of the universe, from bacteria cultures to galaxies to the human body. Spatially speaking, it could provide the information of the length of any curve in real world – the area of, for example, an island or a piece of leaf, the galaxy cluster, the density of matter, and the agglomeration of particles. From the time point of view, one could understand the chemical reactions, population growth, economy, weather, fractal art, and landscapes from the fractal analysis. In the past decades, a number of researches on fractals have been performed; consequently, there have been a variety of the analysis methods (Mandelbrot 1983).

In this paper, we will focus on the fractal analysis on the dissolution process of solid particles and review the fractal reaction as well as the nature of the particles during the dissolution process by collecting and comparing the published results. The methods for analyzing the roughness of the particle surface before and after dissolution will be concluded and a population of particles with a size range will be characterized. The dissolution process as a whole system will be indicated by fractal as well.

2 Fractals and dimensions

2.1 Concept of fractals

To describe the structure of space, the classic geometry as pioneered by Euclid was fundamental on three postulates: (1) the space does not have holes or boundaries, (2) the space is homogeneous and isotropic, and (3) the space is flat and has no intrinsic curvature (Penrose 2005). Generally, many patterns of nature are too irregular and fragmented to agree with the Euclidean theory. These patterns challenged researchers to study the forms left by Euclid to investigate the morphology of chaos. The term "fractal," which is derived from the Latin word "fractus" meaning broken or fractured, was coined by Mandelbrot to indentify a family of shapes. It was a new geometry of nature to describe many of the imperfect objects and lead to full-fledged theories (Mandelbrot 1983).

The roots of mathematically rigorous treatment of fractals can be traced back to functions studied by Georg Cantor who represented the Cantor set in 1883 (Levenspiel 1972, Mandelbrot 1983, Mortimer and Taylor 2002), Waclaw Sierpinski who introduced the Sierpinski gasket and carpet in 1916 (Birdi 1993, Peitgen et al. 2004, Stós 2006, Cristea and Steinsky 2010), and Helge von Koch who invented the Koch curve in 1904 (Birdi 1993, Peitgen et al. 2004, Milosevic and Ristanovic 2007, Paramanathan and Uthayakumar 2010). Besides, there are some other basic fractal models, such as the Peano curve, the space-filling curves, discovered by Giuseppe Peano in 1890 (Kennedy 1974, Sprecher and Draghici 2002), the Hilbert curves and RBG curves presented by David Hilbert (Liu 2004, Chen and Chang 2005), and the Julia sets proposed by Gaston Julia (Kameyama 1993).

To obtain the constructions of the models, taking Koch curve as an example (Figure 1), one first starts with a single line. This initial shape object is the "initiator." Partition it into three equal parts. Then replace the middle third by an equilateral triangle and take away its base. This new form is called the "generator" because it specifies a rule that is used to generate a new form. One continues to repeat, taking each of the resulting segments, partitioning them into certain equal parts and deleting the middle. Self-similarity is built into the construction process. The constructions are all fundamental on an equation that undergoes iteration, a form of feedback based on recursion.

Literally, self-similarity means that a figure, the motif, keeps repeating itself on an ever-diminishing scale. Mandelbrot (1983) proposed the concept of "self-similarity" as the fractal invariant, which must be modified and/or restricted in its scope under both displacement and change

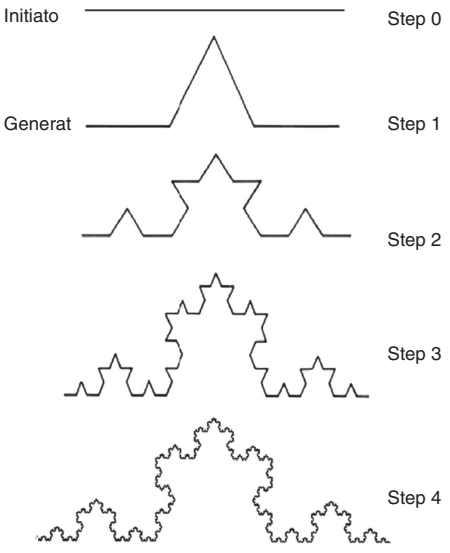

Figure 1 Construction of the Koch curve proceeds in stages. In each stage, the number of line segments increases by a factor of 4 (Peitgen et al. 2004).

of scale. The invariant under certain transformation of scale is called "scaling." While the term fractal points to disorder and covers the cases of intractable irregularity, the modifier scaling points to a kind of order. Alternatively, taking scaling as the primary term pointing to strict order, fractal is a modifier meant to exclude lines and planes.

It can be concluded that the fractal models have the following common features (Falconer 1990): (i) it is self-similar, at least approximately or stochastically; (ii) it has a fine structure, that is, it contains detail at arbitrarily small scales; (iii) it has a straightforward and recursive definition; (iv) it is too irregular to be easily described in traditional geometric language, because it is not the locus of the points that satisfy some simple geometric condition, nor is it the set of solutions of any simple equation; and (v) its size is not quantified by the usual measures such as length.

2.2 Fractal dimension

The concept of dimension has various mathematical connotations, the most common of which is known as the topological dimension. The dimension is known as the integer number, namely 0, 1, 2, and 3, which indicate the point, line, plane, and space, respectively. However, fractals that are irregular geometric objects require a new meaning of dimension. According to Mandelbrot's definition (Mandelbrot 1983), one selects an arbitrarily small measurement unit a, the yardstick. Then, one measures the length of the

meandering line by approximating it as close as possible with a bent line made up of equal line-segments of length a. Supposing the yardstick is used N times, the total length measured is Na, and then the fractal dimension is defined as (Mandelbrot 1983, Lauwerier 1991)

$$D=\frac{\log N}{\log\left(\frac{1}{a}\right)}, \tag{7}$$

or, equivalently,

$$N=\left(\frac{1}{a}\right)^{D}. \tag{8}$$

As discussed above, Na is the total length measured, and the length of curve L is formulated as

$$L=\left(\frac{1}{a}\right)^{D-1} \tag{9}$$

which shows clearly once again how the length measured increases as the measuring unit decreases.

For the Koch curves in Figure 1, if the base has length 1, the curve at Step 1 will consist of four line-segments, of length 1/3 each. The total length consequently will be 4/3. On the next step, each one of the four line-segments is taken as a base and replaced by the corresponding scaled-down curve. The result will be a bent line consisting of 4×4=16 line-segments (Step 3) and having a total length of $(4/3)^2$ or 16/9. Similarly, the third step in Figure 1 produces 4^3=64 line segments of length $(1/3)^3$=27 each (Lauwerier 1991). Therefore, one can obtain a set of curve lengths with the length of segment and the corresponding times N:

$$\begin{array}{lllll} a & 1, & 1/3, & (1/3)^2, & (1/3)^3, \ \ldots \\ L & 1, & 4/3, & (4/3)^2, & (4/3)^3, \ \ldots \\ N & 1, & 4, & 4^2, & 4^3, \ \ldots \end{array}$$

The fractal dimension D could be taken from the slope of log(1/a) versus log(L) or log(N). As shown in Figure 2, we find that the D value is 1.26, the same result obtained from D=log(N)/log(1/a)=log(4)/log(3).

If a solid has a fractal surface, many physical properties depend not only on the fractal dimension but also on the scaling behavior of the entire solid and of the pore space. Thus, environmental particles can be characterized in terms of the fractal dimension of the surface (surface fractal dimension, D_s), fractal dimension of mass (mass fractal dimension, D_m), or fractal dimension of pore (pore fractal dimension, D_p) (Avnir 1989, Huang et al. 1998). The fractal objects based on the characteristics of the three

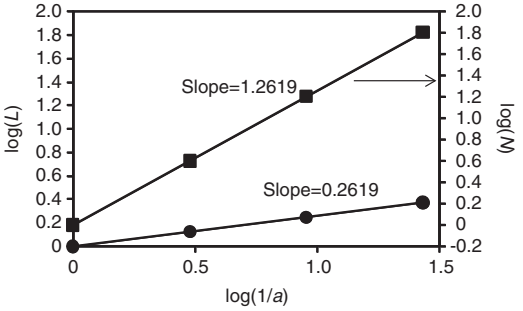

Figure 2 Relation of log(1/a) versus both log(L) and log(N) for Koch curves.

fractal dimensions above are classified in Table 1 (Pierre 1987). As shown in Figure 3 (Avnir 1989), the system is called a mass fractal when mass and surface scale alike; it is called pore fractal if pore space and surface scale alike; the system is called a surface fractal, if only the surface is fractal. Similarly, the distribution of the reactive site on the surface of soil particles may be treated in the same way (Huang et al. 1998), and a reactive fractal dimension D_R may be assigned when the scale of chemically active sites is alike to the surface scale.

3 Fractal nature of particles in dissolution process

3.1 Change in surface geometry during dissolution

Surface geometry is of considerable importance to the heterogeneous reaction. In general, the surface is described by the specific area of the particle, which might be the available area to the solid-liquid reaction. The specific surface area and the shape are related to grain size and repartition (Boldyrev et al. 1979). The superficial reaction of a particle

Table 1 Classification of fractal objects based on D_s, D_m, and D_p (Huang et al. 1998).

Classification	D_s	D_m	D_p	Characteristics
Surface fractal	D	d	d	Only interface is fractal (Figure 3A).
Mass fractal	D	D	d	Interface and the object itself are fractal (Figure 3B).
Pore fractal	D	d	D	Interface and pore structure are fractal (Figure 3C).

D, fractal dimension of the object; d, Euclidean dimension of embedding space.

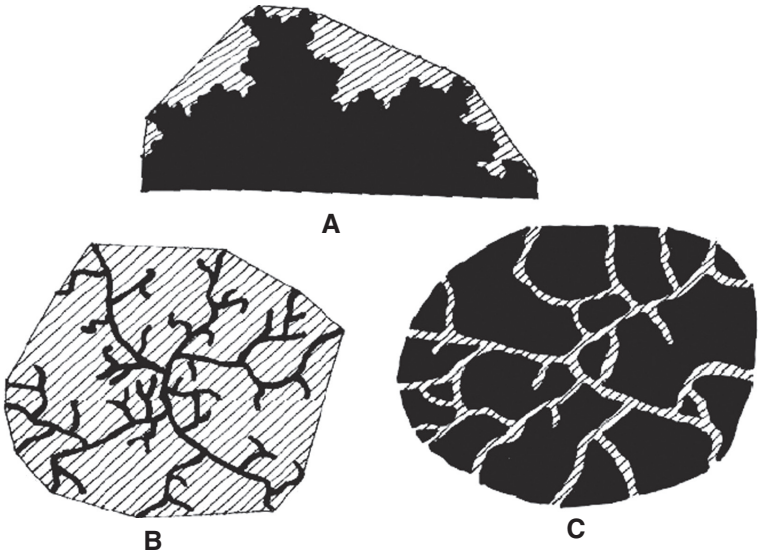

Figure 3 Two-dimensional representations of (A) surface fractal (represented by the border line), (B) mass fractal (represented by the dark area), and (C) pore fractal (represented by the white area) (Avnir 1989).

starts with a very slow overall reaction rate and gets to a stable rate later. The impurities of the surface are important to the initial step. However, if the starting particles are imperfect crystals, they react at high rate first and are subsequently attacked at a slower rate (Avnir 1989).

When leaving the particles in a solution where the reaction takes place, the surface geometry will change more or less after some time. On the one hand, the superficial roughness (specific surface area) alters while the particles dissolve in solution. A study on the two types of calcite, namely, micrite grains and sparite crystals dissolving in acidic water, showed that both the geometric and the reactive surface area changed (Noiriel et al. 2009). The micrite reactive surface area exhibited parabolic changes, whereas that of sparite greatly increased with time. The overall geometric surface area decrease and the pore size increase of the sparite crystal resulted from the pore smoothing and connectivity increase.

Xu et al. (2009) used an index, surface roughness factor, which is the ratio of the Brunauer-Emmett-Teller (BET) specific surface area to the geometric surface area, to characterize the change of the morphology of the reacted quartz. After reacting in a caustic-carbonate solution, the roughness factor of quartz particles increased rapidly with the reaction time at 250°C. The results were confirmed by the scanning electron microscopy (SEM) images of the starting and reacted quartz, the starting particles having some small pits and cracks as well as a reasonably smooth surface and the reacted ones being full of rough etch pits.

The marble grain dissolution at alkaline pH investigated by Orkoula and Koutsoukos (2001) showed that the surface properties remained unchanged at low extents of dissolution, whereas significant alterations took place with a further loss of mass. The specific surface area and mesoporosity decreased in the extent of 2–30% dissolution, and the macropores appeared to grow in size, suggesting that the smaller pores give way to larger ones through dissolution in the interior and/or through merging to yield pores of larger size.

Hailin et al. (1993) studied the relationship of dissolution rates during hornblende dissolution at pH 4.0 to surface. During the early stages of reaction, the specific surface area and surface roughness ratio increased rapidly, while there was a little change in the specific surface area with continued reaction. The formation of etch pits and preferential dissolution along cleavage planes accounted for the increased surface area and increased surface roughness ratio, which was indicated from SEM and N_2 adsorption.

The surfaces of quartz grains after dissolving in atmosphere-equilibrated deionized water at 200°C were analyzed by Gautier using SEM (Gautier et al. 2001). The SEM images revealed that etch pit appeared on the grain surfaces as dissolution progresses, leaching to the significant measurement BET surface area increases.

Grandstaff studied the changes in surface area and morphology of forsteritic olivine dissolution in buffered solution containing sodium acetate and acetic acid (Grandstaff 1978). The specific surface area of the grains increased by a factor of 7 in the first 100 h of the dissolving experiment. As shown by the SEM images, the surface of a grain prior to dissolution appeared as two poorly

developed cleavages, whereas the surface was altered markedly after dissolution, in some of which the edges created by intersecting cleavage surfaces were extensively rounded, but in some of which the large solitary etch pits developed along individual structural discontinuities or at the intersections of discontinuities.

The surface features of welded tuff before and after aqueous dissolution observed with SEM were that a porous matrix surface and fractures are apparent on the surface of the unreacted grain and the etched grain, tuff reacted in 0.01 M HCl had a slightly greater surface texture and apparent porosity than the unreacted tuff, the surface of tuff was reacted in 0.1 M HCl altered markedly, and the etch pits and particulates were visible on the grain surface (Reddy and Claassen 1994).

On the contrary, the particle size distribution (PSD) changes with time as a result of the difference of the reactivity of particles of different sizes and shapes. In Xu et al.'s study on quartz grains reacting in a caustic-carbonate solution, the uniform particle size transformed from 231 μm to a size range revealed by a bimodal curve after the initial quartz dissolving at 250°C for 5 min (Xu et al. 2009). Orkoula and Koutsoukos (2001) observed that the particle size changed dramatically only at a high extent of dissolution when marble particles dissolve in an alkaline solution. The smaller particles disappeared, while the larger decreased in size due to dissolution and/or fragmentation.

3.2 Fractal analysis of superficial roughness

Most of the geometries one encounters in the dissolution process are so disordered and complex that the geometric problem appears not only in the evaluation of the degree of irregularity but also in the evaluation of the degree of the heterogeneity in the surroundings. It is worth applying fractal to describe the roughness of particles. There are various methods used for the fractal analysis of roughness, which are all based on the determination of the number of objects of a given size required to cover the surface.

3.2.1 Boundary fractals of profiles

The fractal dimension can apply to a line with fractal dimension D_l as well as to a surface with D_s, related to D_l as follows (Thibert et al. 1988, Avnir 1989, Farin and Avnir 1992):

$$D_s = D_l + 1. \tag{10}$$

While D_l is experimentally determined, D_s is a derived parameter. The range of values of a fractal dimension depends on the nature of the geometric parameter considered that D_l is between 1 and 2 and D_s is in the value range of 2–3. Within the range considered, the more irregular and rough an object is, the higher is the fractal dimension (D_l and D_s) value.

A straightforward technique for measuring the fractal dimension of the rough surface with rugged profile is to use what is known as the structured walk technique. In this technique, one constructs a polygon of side length λ by exploring the perimeter with a set of compasses set to a distance λ. The perimeter of the profile at a resolution λ is $P=(m+\alpha)\lambda$, where m is the number of steps around the profile and $\alpha\lambda$ is the length of last step that is less than λ. If the boundary is a fractal, a graph of perimeter estimates P versus λ generates a straight-line relationship, the slope of which is related to the fractal dimension by formula (Kaye 1986, Farin and Avnir 1992)

$$P = \lambda^{1-D_l} \tag{11}$$

where D_l is the fractal dimension of the boundary. The fractal dimension of the particle contour can be calculated from the slope of Richardson plot, that is, the natural logarithm of perimeter length P versus the natural logarithm of step length λ.

SEM is the regular method to select different step lengths. At the highest magnification chosen, SEM automatically selected a smallest step length for the measurement of the perimeter. The fractal analysis relies on the fact that the perimeter of a silhouette edge is dependent on the step length with which it was measured. The smaller the step length is, the larger is the perimeter measured, because more details of the structure are taken into account (Thibert et al. 1988). Decreasing the magnification therefore decreases the resolution power of SEM, and a longer step is thus used to measure a shorter perimeter. The operation is repeated for several times until a magnification is so low that the resulting data lack measuring.

Fernández-Hervás et al. (1994, 1996a) applied SEM to characterize the particle morphology of diclofenac hydroxyethylpyrrolidine salt before and after thermal treatment. Similar fractal dimension values were yielded. Besides, Fini et al. (1996) first applied the same procedure to investigate the irregularity degree of the surface of sodium cholate particles. The D_s values of both the crystallized and commercial samples were found, the low D_s obtained in the case of the crystallized sample is very similar, and the commercial sample after sieving has a high D_s within a relatively large range of 2.7–2.96. Then,

they obtained the surface fractal dimension of six salts of ursodeoxycholic acid (Fini et al. 1998).

Kaye et al.'s work revealed the application of the perimeter method to describe the changes in fractal structure of the aluminum shot fineparticles on the partial dissolution by hydrochloric acid. The outline of the particles taken at different eroding stages were drawn and the contour line was characterized by fractal dimension D_l, showing two types of changes. On the one hand, the fractal dimension appeared to drop initially, as any superficial protuberances were dissolved but then increased as erosion bites into the main body of the fineparticle. On the other hand, the composite profile might break into two. It could be seen that again initially the acid cleaned up the profile with a fractal dimension dropping, but then the fractal dimension of the overall profile increased until the breakup of the agglomerate. The smaller fragment was initially of lower fractal dimension, but again this increase gradually (Kaye et al. 1985).

Fini et al. (1998) suggested that the use of this method that examines a group of particles with SEM micrographs of the particle surface is possible to validate the surface fractal dimension with the starting of D_l. However, several limitations of such a method to describe the roughness of particles were found by Anvir: (1) many details hiding in the inner section are ignored because it is a two-dimensional projection and not a cross-section and (2) the Richardson plot result is problematic in the case of D_l <1.2 (Avnir 1989).

3.2.2 Molecular adsorption

3.2.2.1 Monolayer adsorption based on the size of adsorbate molecule

To define the irregular surface area with cracks and fissures, one uses a kind of yardstick. It is noted that the concept of area of irregular objects is not absolute but depends on both the yardstick size and surface properties. Small molecules are usually applied as the yardstick to adsorb on the fractal surface. In principle, the number of moles n of molecules (e.g., spherical ones), forming monolayer on the solid surface, is related to the surface area. If the radius r of covering spherical molecules varies, the dimension of the surface can be taken from a power relationship shown as (Pfeifer and Avnir 1983, Avnir 1989):

$$n \propto r^{-D}. \tag{12}$$

In fact, the adsorbate molecule does not need to be spherical, but the effective cross-sectional area of the adsorbed molecular forming the monolayer σ is the same for all members, which is the geometrical similarity. In that case, Equation (12) turns into (Pfeifer and Avnir 1983, Avnir 1989)

$$n \propto \sigma^{-D_a/2}, \tag{13}$$

where n is the monolayer value (moles per unit mass) and D_a is the surface fractal dimension obtained from the adsorption experiment.

A common method is to divide the surface area from BET method by the monolayer value of the investigated molecule. The procedure is proper only for smooth surfaces, that is, for surfaces of low fractal dimension, in which the available surface area is independent of the probe size. An unfortunate common error is to apply this procedure to highly irregular surfaces for which surface accessibility is strongly dependent on the probe size (Farin et al. 1985).

Hundreds of investigators (Love and Whittaker 1954, Burns and Carpenter 1968, Corn et al. 1973, Urano et al. 1982, Avnir et al. 1983, Farin et al. 1985, Gasparini and Mhlanga 1986, Frank et al. 1987, Friesen and Mikula 1987, Inoue et al. 1988, Kaneko et al. 1989a,b) got access to the fractal dimensions of the surfaces of various particles by employing different molecules, namely, alkanes, alcohols, benzene, dioxane, naphthalene, anthracene, phenanthrene, N_2, Ar, and Kr. One example on the application of Equation (13) is the study of Avnir who summarized the adsorption experiments (Figure 4) on increasingly activated charcoals investigated by Nay and Morrison (1949). The D_a values amplified the progressive changes in the microporous structure. The micropores dominated in charcoal No. 1 with D_a=3.03, while the surface of charcoal

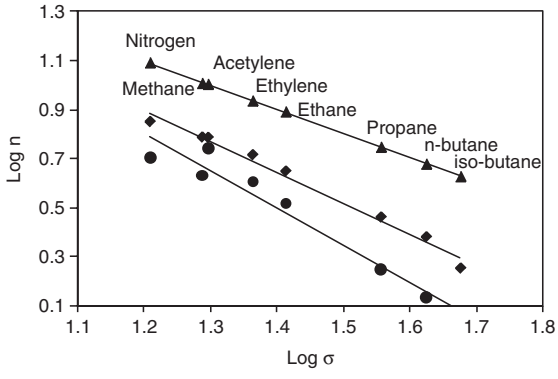

Figure 4 Monolayer amount of adsorbate, n (mmol/g), as a function of adsorbate cross-section σ (Å²), for activated charcoal No. 1 (●, D_a=3.03), No. 3 (◆, D_a=2.54), and No. 8 (▲, D_a=1.94) (Avnir et al. 1983).

No. 8 is free of pores of size in contrast, with D_a dropping to 1.94, implying that the activation smoothens pores.

Avnir et al. concluded and reanalyzed the molecular accessibility dimensions of surfaces as determined from the adsorption data in open papers (Avnir et al. 1984, Avnir 1989). The fractal dimension D_a of most of the particles between 2 and 3 showed the fact that the fractal theory limit of 3 reflects the irregularity of roughness surfaces. $D_a \approx 2$ refers to the smooth, flat area, and $D_a > 2$ values may originate from subsets of even rougher surfaces. However, on the one hand, there is a case of $D_a < 2$, that is, Graphon covered by N_2 and a series of alkanes (C_5–C_{12}) had a fractal dimension of 1.88 (Avnir 1989), which is also interpretable in terms of the fractal dimension to subsets of all surface points. On the other hand, $D_a > 3$, for example, silica-60 with fractal dimension of 3.42 obtained from n-alkane (C_1–C_4) adsorption (Drake et al. 1986), cannot be interpreted in terms of the geometrical dimension because the value is larger than the dimension of the embedding environment, but it exists really and results from the sieving effects (Avnir 1989), chemisorptions (Drake et al. 1986), and the nonfractal distributions of active sites (Farin and Avnir 1988).

However, in terms of the application of Equation (13), several problems exist. The power law is limited in a range that is related to the given set of σ values. The fractal dimension obtained from short-range molecules might be different what is plotted at a supramolecular scale. Only when we assume that just physiosorption is involved in the formation for the monolayer blanket and each kind of molecule is adsorbed on the same line is the effective surface similar for various adsorbates. The process might be change if chemisorption or reaction is involved. Sometimes, there is a high degree of connectivity and/or porosity existing in the object whose specific geometry could not be reflected by the obtained D_a values. Another problem is that it is difficult to assess the cross-sectional value of the molecule correctly because the weakly physiosorbed molecules arrange on the surface with no specific orientation (Avnir 1989).

3.2.2.2 Monolayer adsorption based on the particle size of adsorbent

Another use of the molecules as yardsticks is to determine the change of the reactive and nonreactive surface areas as a function of the object size with a fixed yardstick, where a self-similarity exists both within the same object and between different objects (Avnir 1989).

In practice, it is neither possible nor desirable to exert an adsorption experiment on a single adsorbent granule but on a bulk of particles. In units of moles per volume, the powdered adsorbent, each powder particle with radius R, contains a constant R^3. Therefore, the number of the fixed adsorbate molecules n and the apparent total surface area A vary with the object radius R as (Pfeifer and Avnir 1983, Avnir et al. 1984, Avnir 1989, Farin and Avnir 1992)

$$n \propto A \propto R^{D_r - 3}. \tag{14}$$

Normally, one performs an experiment on a unit mass of particles. To measure the porosity of an object, on extreme is a smooth surface particle, $n \propto R^{2\text{-}3}$ per unit mass. On the other extreme of a highly porous particle, the external area is negligible compared to the internal area, where $n \propto R^{3\text{-}3}$. In other words, the surface area A becomes independent of R. Equation (14) therefore gives a measure of the irregularity degree between these two extremes.

It is easy to get the value of D_r from the Richardson plot of specific surfaces as a function of particle radius. For a bulk of particles, each particle cannot have the exactly same size with others. In this case, one separates the particles into several fractions with a small size range and uses the mean radius to describe the particle size of a population of particles as a whole. One example is shown in Figure 5, taken from the work of Tromelin et al., who determined the surface fractal dimension D_r of an orthoboric acid powder by the adsorption of krypton (Tromelin et al. 1996). The powder was ground and divided into five narrowly sieved fractions. The D_r value was calculated from the slope of the Richardson plot and was found equal to 2.42.

Besides the results concluded by Anvir (Avnir et al. 1983, Farin and Avnir 1987, Avnir 1989), there are other investigations on the surface fractal dimension that are based on the relation between the BET surface area and the mean particle size (Avnir et al. 1985, Farin and Avnir 1992, Fernández-Hervás et al. 1996b, Tromelin et al. 1996,

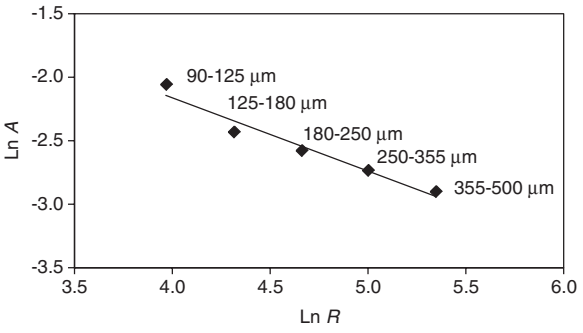

Figure 5 Kr BET surface area versus particle size of granulometric fractions of orthoboric acid powder (Tromelin et al. 1996).

2001). Most of the materials obey Equation (14) and the D_r values obtained were between 2 and 3.

Equation (14) is available in the case of the powder sample having a constant apparent density. In constant, when the density of a bulk of powdered adsorbents is a function of a particle size, the particles are mass fractals with dimension D_m. Equation (14) turns into (Ben Ohoud et al. 1988, Avnir 1989)

$$A \propto R^{D_r - D_m}. \tag{15}$$

Although Equation (15) seems more exact than its original to express the relation between the surface area and particle size of a population of particles, Equation (14) is used routinely, since a wide variety of commercial powders such as oxides, clays, and carbons, in the micron to millimeter range, have D_m=3 according to Damme's investigation (van den Vlekkert et al. 1988, Avnir 1989).

3.2.2.3 Fractal isotherm equation

In practice, there is a case that the number of adsorbed molecules is much larger than the number to form a monolayer, named as multilayer adsorption. For example, the IV-type adsorption-desorption isotherm in the BDDT classification suggests that the adsorption occurs by the monolayer-multilayer mechanism at low and medium relative pressures and by the capillary condensation at high relative pressures (Sahouli et al. 1997). Pfeifer et al. extended the classic Frenkel-Halsey-Hill (FHH) theory of multilayer adsorption on a flat surface to fractal surface in the following form (Pfeifer et al. 1989a,b):

$$\ln\frac{N}{N_m} = s\ln\left(-\ln\frac{P}{P_0}\right) + C_1, \tag{16}$$

where N/N_m represents the fractions of surface coverage, P and P_0 are the equilibrium and saturation pressure of the adsorbate, respectively, C_1 is the intercept, and the parameter q is related to the surface dimension of the sample. It is noted that there are two possible adsorption regimes to determine the surface fractal dimension $D_{s,\mathrm{FHH}}$. When the van der Waals attractive forces govern the formation of the adsorbed film, which tends to make the gas-film interface to replicate the surface roughness, the $D_{s,\mathrm{FHH}}$ value is obtained as (Jaroniec et al. 1997)

$$D_{s,\mathrm{FHH}} = 3(1+s). \tag{17}$$

On the contrary, if the liquid-gas surface tension (capillary force), which tends to move the interface away from the surface to reduce the interface area, is more important, the $D_{s,\mathrm{FHH}}$ is estimated by (Jaroniec et al. 1997)

$$D_{s,\mathrm{FHH}} = 3+s. \tag{18}$$

In Equation (16) of the fractal FHH equation, the parameter s surface fractal dimension can be obtained from the slope of the $\ln(N/N_m)$ versus $\ln[-\ln(P/P_0)]$, and the surface fractal dimension thus is calculated by Equation (17) or (18). For most cases, the plot exhibits a linear portion at higher coverage, but a strong curvature is, in general, observed below or near a monolayer coverage. The fractal isotherm equation can only be applied within a range of the fractional coverage (Kaneko et al. 1991). Pfeifer and Cole (1990) suggested that the fractal FHH model was valid at high relative pressures when capillary condensation is the dominant mechanism. Neimark proposed that P/P_0>0.7 (Neimark 1990a,b,c) and P/P_0 ranged from 0.7320 to 0.9826 according to Wang et al.'s study (Wang et al. 2007). The P/P_0 range applied by El Shafei et al. for a set of samples heated under various temperatures varied from 0.15 to 0.90 to from 0.05 to 0.4 (El Shafei et al. 2004).

Since $2 \le D_{s,\mathrm{FHH}} < 3$, Equation (17) predicts $-1/3 \le s < 0$, but Equation (18) suggests one should have $-1 \le s < 0$. It has been argued that when s=-1/3, corresponding to a $D_{s,\mathrm{FHH}}$ of 2 by Equation (17) and $D_{s,\mathrm{FHH}}$=2.67 by Equation (18), the increase of adsorption resulting from the capillary condensation is exactly compensated by the reduction of the adsorption space due to the fractal characteristic of the surface. It follows that the value of $D_{s,\mathrm{FHH}}$ cannot be unambiguously determined from a single adsorption isotherm when $s \ge -1/3$. In this case, the desorption should also be measured to ensure the presence of capillary condensation within mesopores (Pfeifer and Cole 1990, Lee and Tsay 1998). The surface fractal dimension $D_{s,\mathrm{FHH}}$ can be estimated from the desorption data by using (Jaroniec et al. 1997, Wang et al. 2007)

$$\ln\frac{N}{N_m} = (D_{s,\mathrm{FHH}} - 3)\ln\left(-RT\ln\frac{P}{P_0}\right) + C_2 \tag{19}$$

where the relative pressure P/P_0 is more than 0.53 and C_2 is the intercept constant.

In addition to the fractal FHH equations discussed above, Neimark (1990b) proposed a so-called thermodynamic fractal isotherm equation relating the area of the gas-liquid interface S and the mean radius of the curvature of this interface r' by the equation

$$\ln S = C_3 - (D_{s,T} - 2)\ln r' \tag{20}$$

where C_2 is the intercept constant. The surface fractal dimension can be estimated from the slope of the regression in Equation (20) at relative pressure ranging from 0.7320 to 0.9862 (Wang et al. 2007). The model reflects the idea that, during the adsorption on a fractal surface, the surface is smoothed by the adsorbate, and the surface of the adsorbent covered with an adsorbate is smaller than the surface of the uncovered adsorbent (Wang et al. 2007).

In this equation, the area of the gas-liquid interface S can be calculated according to the Kiselev equation:

$$S=\frac{RT}{\gamma}\int_{N(P/P_0)}^{N_{\max}}(-\ln x)\,dN \tag{21}$$

where $N_{\max}$ denotes the amount adsorbed when P/P_0 approaches unity and γ expresses the liquid tension. The Kelvin equation is used to convert the equilibrium pressure to the mean radius of the curvature.

Wang and Li (1997) found that neither the FHH equation or the thermodynamic method yielded accurate estimates of the fractal dimension of porous media under the whole range of experimental scales and proposed the modified thermodynamic model that accounted for the effect of the volume encompassed by the liquid-gas interface in the process of capillary condensation. The modified model is expressed as follows:

$$\ln A\left(\frac{P}{P_0}\right)=C_4+D_{s,\mathrm{MT}}\ln B\left(\frac{P}{P_0}\right) \tag{22}$$

where

$$A\left(\frac{P}{P_0}\right)=\frac{-\int_{N_{P/P_0}}^{N_{\max}}\ln\frac{P}{P_0}dN}{r'^2}\quad\text{and}\quad B\left(\frac{P}{P_0}\right)=\frac{(N_{\max}-N_{P/P_0})^{1/3}}{r'}$$

C_4 denotes the intercept constant.

Besides, another model, developed by Mahnake and Mögel based on the BET formula, is used to determine the fractal dimension of a surface from one adsorption isotherm (Mahnke and Mögel 2003). An alternate derivation is suggested to avoid the inconsistent behavior in the case of a surface fractal dimension of 3. The model is formulated as

$$\ln\frac{V_{(P/P_0)}}{V_m}=\ln\frac{c(P/P_0)}{1-(P/P_0)+c(P/P_0)}-(3-D_{s,\mathrm{MM}})\ln(1-P/P_0) \tag{23}$$

where $V_{(P/P_0)}$ and V_m denote the volume of gas adsorbed at P/P_0 and in monolayer, respectively, and c is the constant estimated by the Mahnake and Mögel formalism.

The analyses of many surface science reports (Table 2) followed by the experiments specially designed to test the fractal approach have revealed that, in most cases, the application of Equation (17) yields the value of D_s smaller than 2 that is physically meaningless for a surface dimension. Equation (18) combined with Equation (16) has been extensively used to evaluate the fractal dimension for various samples. To some extent, the fractal dimension derived from the adsorption data approximates to the values calculated by using the desorption data on the same isotherm, no matter which model is used. The D_s value by thermodynamic model usually approaches to 3, higher than the values from other laws, and is more than 3 in some special case giving a nonmeaningful indication for particle surface irregularity (Wang et al. 2007).

3.3 Fractals of PSD

In the real dissolution process, the particles, such as the mineral ore and the drug tablets, do not actually exist as a uniform particle size but instead as a distribution of particle sizes. Therefore, the particle size might be stochastic during the dissolution process where the rate that depends on the particle diameter is correspondingly random. It is questionable to express the total sample of particle size by a single value.

Figure 6, which is taken from the investigation of Mihranyan et al. (2009), who studied the dissolution process of sparingly soluble calcium carbonate, reveals that the PSD was altered during the dissolution for $CaCO_3$ particles. It is obviously seen that the peak of size distribution shifted gradually toward smaller particle sizes until it stabilized after 24 h of dissolution and remained unchanged.

3.3.1 Single fractal model

A power-law relation between the number and size of objects has been proposed (Turcotte 1986)

$$N(R>r)=cr^{-D_d}, \tag{24}$$

where $N(R>r)$ is the number of objects per unit volume having a radius R larger than r, C is a constant of proportionality, and D_d is the PSD fractal dimension.

Tyler and Wheatcraft noted that it was more convenient to express, in practice, the mass-based power law than the number-based power law to estimate the fractal dimension (Scott and Wheatcraft 1992):

Table 2 Multilayer fractal dimensions of surfaces as determined from adsorption-desorption isotherm.

Adsorbent	Fractal FHH isotherm equation		Neimark's thermodynamic model	Modified thermodynamic model	Mahnake model	References
	$D_{s,FHH}$ value by Equation (18)	$D_{s,FHH}$ value by Equation (17)	$D_{s,T}$ value	$D_{s,MT}$ value	$D_{s,MM}$	
Alumina calcined below 1200°C	2.50–2.60	1.51–1.79	2.41–2.99	2.41–2.99	2.40–2.83	Lee 1998, Lee and Tsay 1998
				2.29–2.88[a]	2.30–2.57[a]	
Alumina calcined at 1250°C	2.80/2.68	2.38/2.05	2.32/2.86			Lee and Tsay 1998
3 γ-Al_2O_3 samples				2.66–2.75		Wang and Li 1997
				2.75[a]		
Alumina borate calcined below 1200°C	2.51–2.63	1.51–1.90	2.27–2.86	2.27–2.86	2.26–2.69	Lee 1998, Lee and Tsay 1998
				2.27–2.80[a]	2.24–2.54[a]	
Alumina borate calcined at 1250°C	2.70/2.67	2.07/2.02	2.47/2.86			Lee and Tsay 1998
CaHap calcined below 900°C	2.40–2.65	1.20–1.95	2.43–2.96			El Shafei et al. 2004
CaHap calcined at 900°C	2.14	0.33	3.00			El Shafei et al. 2004
MgO samples			2.43–2.55	2.33		Wang and Li 1997
			2.36–2.54[a]	2.41–2.51[a]		
TiO_2-ceramic UF membrane			2.49		2.3	Mahnke and Mögel 2003
5 samples including soil particles and sediments	2.69–2.80		2.99–3.1			Wang et al. 2007
	2.69–2.82[a]					
Calcined ZrO_2-Y_2O_3 nanopowder at different temperatures (400–900°C)	2.50–2.60		2.42–2.54			Gurnyk et al. 2010
Amberlite XAD-4 (macroporous polymer)	2.71					Li et al. 2010
HPA-1 (hypercrosslinked polymer)	2.47					Li et al. 2010
12 coal samples	2.36–2.58					Liu et al. 2010
Chinese coal samples	2.35–2.73	1.05–2.19				Yao et al. 2008
	2.44–2.85	1.31–2.56				
Triblock copolymer mesoporous silicates calcined between 300°C and 900°C	2.52–2.72	2.02–2.40	2.58–2.72			Smith and Lobo 2010
A variety of dehydroxylated silica	2.17–2.56[b]				2.14–2.66	Watt-Smith et al. 2005
	2.51–2.70				2.31–2.66	
CuO/Al_2O_3 catalyst			2.14–2.39		2.24–2.44	Rozic et al. 2006
Pt/TiO_2 catalyst pretreated from 300°C to 900°C			>2.58		2.20–2.39	Peng and Wang 2007
Carbon electrode materials	2.56–2.80				1.90–2.81	Watt-Smith et al. 2008
Carbon black samples	2.54–2.59	1.64–2.07	2.38–2.59			Sahouli et al. 1997, 1999
Activated carbon	2.98	2.96±0.01				
Carbons synthesised using silica template	2.51–2.66					Lee and Pyun 2005
Carbon nanotubes			2.51–2.58			Hou et al. 2005
Carbon fibers	2.60–2.71					Kaneko et al. 1991
Acid-activated bentonites					2.11/1.94	Rozic et al. 2008
Mesoporous silica prepared under various synthesis conditions	1.85–2.92					Prouzet et al. 2009
Silica particles obtained in emulsion and microemulsion media	2.49–2.99		2.42–3.3	2.32–2.78		Esquena et al. 2000

(Table 2 Continued)

Adsorbent	Fractal FHH isotherm equation		Neimark's thermodynamic model	Modified thermodynamic model	Mahnake model	References
	$D_{s,FHH}$ value by Equation (18)	$D_{s,FHH}$ value by Equation (17)	$D_{s,T}$ value	$D_{s,MT}$ value	$D_{s,MM}$	
Polybutadiene-coated Li Chrospher Si 300			2.21–2.28			Neimark et al. 1993
Si300			2.22, 2.20[a]	2.34, 2.48[a]		Wang and Li 1997
SiO_2 samples			2.59–2.88	2.41–2.50		Wang and Li 1997
			2.47–2.85[a]	2.53–2.55[a]		
Cement composite	2.50–2.62		2.43, 2.43[a]	2.63, 2.68[a]		Wang and Li 1997; Shih et al. 2006
Porous glass			2.14, 2.10[a]	2.35, 2.52[a]		Wang and Li 1997
Pd-Ag/SiO_2 catalysts	2.25–2.37					Blacher et al. 2000
Frio shale	2.20–2.39		2.50–2.63			Ma et al. 1999
Magnesium trisilicate	2.87–2.93		2.85–2.99			Rizkalla et al. 1999
Magnesium hydroxide	2.42–2.47		2.64–2.73			Rizkalla et al. 1999
Magnesium oxide	2.36–2.53		2.50–2.80			Rizkalla et al. 1999

[a]The fractal dimension obtained from the desorption data.
[b]The adsorbate is C_2H_4, while others derived from the N_2 adsorption-desorption data.

Figure 6 PSD of integral $CaCO_3$ particles after various times of dissolution (Mihranyan et al. 2009).

$$\frac{M(R<r)}{M_T}=\left(\frac{r}{R_{L,\text{upper}}}\right)^{3-D_d}, \tag{25}$$

where R is the particle size, M is the mass of the particles that are larger than a specific measuring scale r, M_T is the total mass, and $R_{L,\text{upper}}$ is the upper size limit for the fractal behavior. The power relation has also a lower limit of validity, $R_{L,\text{lower}}$. The particle radius r of the particles is confined between $R_{L,\text{lower}}$ and $R_{L,\text{upper}}$. It is noted that the mass-based similarity is preserved and the uniform particle density is assumed.

The logarithmic transformation of Equation (25) results in a linear relationship for a scale-invariant PSD:

$$\ln[M(R<r)/M_T]=(3-D_d)\ln r+\ln k \tag{26}$$

where $\ln k=-(3-D_d)\ln R_{L,\text{upper}}$.

The value D_d obtained from the experimental data fitting with Equations (25) and (26) indicates a particular cumulative mass-size distribution and reflects the irregularity of a granular system. On the one hand, the fractal dimension can be applied to describe the fineness of the particles. From Hyslip's work on the size distribution of silty sand-type soil, it is indicated that the higher fractal dimension is, the higher is the relative percentage of fine-grained material with the distribution (Hyslip and Vallejo 1997). Cui et al. (2006) used fractal dimension to study the effect of process parameters on the comminution capability of high-pressure water jet mill and found that the D_d value increased with the increase of the degree of particle comminution. On the other hand, a higher D_d value also suggests a well-graded mixture containing different sizes, while the mixture dominated by particles having a uniform size exhibits a lower value. Lu et al.'s

investigation, on the change in D_d value of Loess formation while comminution time lasting, showed that the larger the value of the fractal dimension was, the wider was the range of particle size (Lu et al. 2003).

To some extent, one estimates the texture of a population of particles from the PSD, because the original object that contains complex compositions (i.e., ores and soils) might be fragmented into random parts due to the intrinsic properties of minerals after treatment such as erosion and dissolution. D_d can therefore indicate the texture of particles. Ersahin et al. (2006) evaluated the fractal dimensions of the PSD for 22 soils with textures, ranging from sandy loam to clay, the values of which ranged from 2.45 to 2.94, showing that finer textures give greater D_d values due to a more complete fragmentation. Liu et al. (2009) and Wang et al. (2006) implied the soil degradation of farmland from the comparison between the fractal dimension of farmland and that of the well-protected forest land. Su et al. (2004) studied 30 types of soils with varying eroding degrees, with the intent of relating D_d to the desertification degree. In the desertification process, the low D_d value indicated the high contents of sand and the serious desertified degree of farmland.

3.3.2 Piecewise fractal model

On the view of the natural organization of the PSDs, it is assumed that there might exist a critical value r_c to partition the whole distribution into two intervals of particle diameter over which the fractal dimensions are different (Millán et al. 2003). The fractal size distribution function in Equation (26) can transform into two sets of parameter model separated by $\ln r_c$:

$$\ln[M(R<r)/M_T] = [(3-D_{d1})\ln r + \ln k_1 (\ln r \le \ln r_c)] + [(3-D_{d2})\ln r + \ln k_2 (\ln r > \ln r_c)]. \quad (27)$$

Equation (27) suggests that the log-transformed data would yield two straight lines to obtain two fractal dimensions, D_{d1} and D_{d1}, from the slops. Each term in parentheses represents a logical operation. The value of r_c can be considered as the upper size of the first domain, the low limit of the second domain. The upper limit of the second interval is just the one of the system size. One example of the application of this equation is the result of Tasdemir, who studied the fractal evaluation of the PSD of chromites. The piecewise fractal analysis of one sample, Bantil ore, shown in Figure 7 (Tasdemir 2009) indicates that the PSD of the first segment with D_{d1}=2.002 is different from the second segment (D_{d2}=2.543).

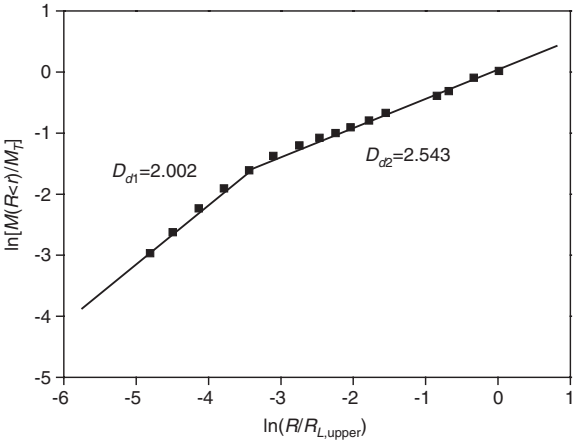

Figure 7 Application of the piecewise fractal model to Bantil ore crushed by hammer (Tasdemir 2009).

Bittelli et al. (1999) characterized the PSDs of 19 soils and found that the whole range of the measurement could not described by a single power-law exponent completely. The PSD curve was divided into three main domains that represented clay, silt, and sand, relating to three fractal dimensions with $D_{clay}<D_{silt}<D_{sand}$. By the same token, Prosperini and Perugini (2008) partitioned the whole PSD of soil samples into two fractal scaling domains and obtained the fractal dimensions ranging from 0 to 3.

Millán et al. (2003) compared the fitness of piecewise fractal model with nonlinear and log-linear regressions by using the experimental data of the PSD for a clay soil and a loam soil (Wu et al. 1993, Bird et al. 2000). The linear regression to log-transformed data showed some lack of fit, as reflected by the low coefficient of determination (0.75), whereas the piecewise law with respect to high correlation (0.98) is regarded to be better.

Single and multifractal methods were applied by Tasdemir to characterize the PSD of comminuted chromite samples (Tasdemir 2009). The employment of the method depended on the degree of energy of comminution applications, in general, the single fractal model being suitable for low-energy events and the piecewise law for the high-energy application. The latter fractal model approach always yields several scaling exponents for the whole domain, which can still describe the irregularity of the size distribution of the particles in the responding portion. As discussed in Section 3.1, the high D_d value monitors the relatively large particle size and the wide size range of the particle domain. It was noted that the transition point from one fractal region to another changed with the type of the ores and comminution conditions. Therefore, from the D_d values, the minerals can be expected to fracture differently

depending on the treating conditions and the mineralogical characteristics. Prosperini and Perugini (2008) also suggested that the power-law domains associated to the fractal scaling of soil particles were directly related to soil textural parameters giving the opportunity to associate the values of multifractal dimensions to the physical attributes of studied samples and allowing the use of fractal statistics as a robust technique to characterize the PSD in samples.

Bao developed a piecewise volume cumulative distribution function with the PSD fractal dimension to express the PSD of natural gibbiste and diaspore particles varying with digesting time. The piecewise fractal model is shown as Equation (28) (Bao 2011, Bao et al. 2013).

$$\begin{aligned} F_V(R>r) = & c_1\left[1-\left(\frac{r}{\lambda_1}\right)^{3-D_{d1}}\right](r_{\min}\le R\le r_{c1}) \\ & +c_2\left[1-\left(\frac{r}{\lambda_2}\right)^{3-D_{d2}}\right](r_{c1}<R\le r_{c2}) \\ & +c_3\left[1-\left(\frac{r}{\lambda_3}\right)^{3-D_{d3}}\right](r_{c2}<R\le r_{c3}) \\ & +c_4\left[1-\left(\frac{r}{\lambda_4}\right)^{3-D_{d4}}\right](r_{c3}<R\le r_{\max}) \end{aligned} \quad (28)$$

where F_V is the cumulative volume of the particles with the size R smaller than r. $F_V(R>r)$ is equal to 1 at the minimum size of the whole size range, $r_{\min}$, and equal to 0 at the maximum size, $r_{\max}$. c_1 and λ_1, c_2 and λ_2, c_3 and λ_3, and c_4 and λ_4 describe the shape and scale for the first, second, and third segments of the cumulative distribution, respectively. D_{d1}, D_{d2}, D_{d3}, and D_{d4} are the PSD fractal dimensions. r_{c1}, r_{c2}, and r_{c3} are the maximum sizes of the first, second, and third segments, respectively. If the cumulative distribution is partitioned into three segments, the fourth item on the right-side of Equation (28) is set as zero automatically and the r_{c3} in the third item is equal the maximum size, $r_{\max}$.

The piecewise fractal model is evaluated by the nonlinear regression analysis to obtain the PSD dimension of the natural particles during the leaching process with various conditions. The outcomes are revealed in Table 3.

4 Approach to fractal dimension of dissolution

4.1 Reactive surface area

The reactive surface area is an important parameter, because the particle-solution interface partially controls the kinetic behavior in many systems. The characterization of the reactive surface area changes resulting from dissolution is a prerequisite to the accurate modeling of the reactive transport in porous media. Considering the mass transfer being steady state, the dissolution rate possibly changes with the variation of the reactive surface area as the chemical reaction process.

However, it is difficult to measure the absolute size of the reactive surface area in practice, because the dissolution rate of the elements in samples might change during the dissolving process due to the variation of the dissolution environment, such as the pH value and saturation. That is why a number of models that described the dissolution process were based on the total surface area measured by the gas adsorption (Brunauer et al. 1938) or the geometrical constructions (Lichtner 1988, Canals and Meunier 1995, Le Gallo et al. 1998, Colón et al. 2004, Emmanuel and Berkowitz 2005) or other methods (Fredrich et al. 1993, Shiraki et al. 2000, Lüttge et al. 2003, Noiriel et al. 2004), such as vertical scanning interferometry, atomic force microscopy, laser confocal microscopy, or X-ray tomography.

The subsequent doubt on the application of the total surface area substituting for the effective reactive surface area appeared (Gautier et al. 2001, Hodson 2006). The initial BET specific surface area could integrate the different dissolution rates and areas of the edge and basal surface. With the dissolution proceeding, the grain edge turned around and etch pits were formatted, since the rate of dissolution on the grain edge was much higher than that on the basal surface. Etch pit walls rapidly evolve into unreactive negative faceted forms where the etch pit density and diameter seemed unchanged during the course of the experiment. The reactive surface area was manifested as a high density of deep cracks running across the coarse grains after dissolution, which did not influence significantly the release of bulk elements into the solution due to the relatively small area of these sites (Hodson 2006). Therefore, although the measured BET surface areas increased with the amount of elements dissolved, the dissolution rates remained constant. It is noted that the unreactive etch pit walls are a part of the bulk of the measured increasing BET specific surface area (Gautier et al. 2001).

Nonetheless, a variation of the reactive surface area could be determined during the dissolution experiment. Colón et al. (2004) used the quotient of dissolution rates at the onset of the dissolution experiment and after an elapsed time to index how the reactive surface area changed. The higher ratio value is, the greater variation took place. Noiriel et al. (2009) proposed a linear

Table 3 PSD fractal dimension of natural gibbsite/diaspore particles in leaching process analyzed by Equation (28) (Bao 2011).

Particle	Leaching condition			PSD fractal dimension			
	C^0_{NaOH} (M)	Temp (°C)	Time (min)	D_{d1}	D_{d2}	D_{d3}	D_{d4}
Nature gibbite particle	0	0	0	2.7921	2.7424	2.9978	0
	2	70	2	1.8181	2.9923	2.9999	0
			5	1.8391	2.9763	2.9990	0
			10	1.9502	2.9648	2.9943	0
			20	1.8865	2.9865	2.9994	0
			60	1.9454	2.9908	2.9991	0
			300	2.0216	2.9846	2.9983	0
	1	90	2	2.0490	2.9471	2.9719	0
			5	1.9933	2.9434	2.9722	0
			10	1.9488	2.9673	2.9882	0
			20	1.9533	2.9689	2.9852	0
			60	1.9542	2.5959	2.9982	0
			300	2.0023	2.4320	2.9995	0
	2	90	2	2.0969	2.9514	2.8870	3
			5	1.9840	2.9912	2.9997	0
			10	2.0304	2.9914	2.9991	0
			20	2.0131	2.9752	2.9967	0
			60	1.8473	2.9994	2.6003	3
			300	1.6173	2.9891	1.8917	2.9999
	3	90	2	1.9040	2.9668	2.9953	0
			5	1.9176	2.9450	2.9902	0
			10	1.8602	2.9813	2.9993	0
			20	1.8962	2.9702	2.9992	0
			60	1.8696	2.9809	2.9997	0
			300	1.9259	2.9816	2.9995	0
Natural diaspore particles	0	0	0	2.5550	2.9588	2.9890	0.0000
	4	240	15	1.9327	2.8689	2.9959	2.9985
			30	2.1357	2.8941	2.9724	2.9871
			60	2.3997	2.6869	2.9864	2.9845
			120	2.3268	2.9571	2.9492	2.9999
			300	2.2307	2.7176	2.9997	2.9989
	6	240	15	2.1944	2.9674	2.9968	2.9992
			30	2.2873	2.9464	2.9951	2.9999
			60	2.3307	2.8132	2.9887	2.9951
			120	2.5237	2.7589	2.9886	2.9857
			300	1.4823	2.8249	2.9878	0

equation set of the fraction of the reactive surface area and dissolution concentrations of elements that were experimental data derived from two types of limestone containing both Ca and Sr. The fraction of reactive surface area was represented as the proportion of the grain surface area that contributed to the chemical reaction, standing for the capability of each mineral releasing the elements. Gouze and Luquot (2011) pointed out that the solid-liquid interface area deduced from the X-ray microtomography (XMT) could not measure the surface area of the reaction directly, but reactive surface area was possibly indexed by the difference between the interface area obtained from XMT acquisitions before and after dissolution, which is proportional to the difference in the reactive surface area before and after an elapsed dissolving time.

4.2 Reactive fractals

The course of a heterogeneous chemical reaction is an outcome of a complex interplay between the details of the chemistry and the details of the irregular and convoluted geometry found in many of the reactive supports. Thus, the fractal phenomenon is not only on the apparent surfaces but also on the conjugated reactive surface. The impact factors including the temperature, concentration, and stirring speed, which dictate the chemical reactivity

(i.e., the dissolution rate during dissolving process) of a fractal object, are both numerous and difficult to separate. To describe the general influence, it is possible to find an indicator, the reaction dimension D_R, which is simply defined as the effective fractal dimension of the object toward a reaction but is the experimentally derived value in many cases (Farin and Avnir 1987, Avnir 1989). It is necessary to note that this fractal dimension is not strictly based on fractal geometry consideration but on a process of reaction or dissolution or a combination of both.

It is noted that the experimental details and the nature of the reaction could be taken as originating from diffusion to and not on the surface. The effective reactive surface is considered as another irregular surface, the area of which indicates the collection of all the sites where dissolution takes place. Similar with the total fractal surface area, the area of the reactive surface could be expressed by the fractal dimension D_R. Farin and Avnir (1987, 1992) proposed two forms of equations according to the Wenzel's law, which describe that the reaction rate is proportional to the reactive surface area. One form in terms of the relation between the irregular surface area and the grain radius is formulated as (Farin and Avnir 1987)

$$-dQ/dt = k_1 R^{D_R - 3}. \quad (29)$$

In addition, a modification of the Noyes-Whitney equation was used to estimate the D_R value based on the mass diameter relation following the classic $Q \propto R^3$ modified (Farin and Avnir 1992):

$$-dQ/dt = k_2 Q^{D_R/3}(Q_e - Q_0 + Q) \quad (30)$$

where Q, Q_e, and Q_0 are the weight of the sample necessary to saturate the solution, the initial weight of the sample, and the weight of the undissolved sample after time t, respectively. $-dQ/dt$ denotes the reaction rate, and k_1 and k_2 are constants dependent on the hydrodynamic conditions.

Equations (29) and (30) are widely used to estimate the D_R value in the dissolution process (Table 2). One example of using Equation (29) is the estimation of D_R values of both commercial and recrystallized sodium cholate particles dissolving in pure water at room temperature (Figure 8), as studied by Fini et al. (1996), who measured the dissolution rate of the six fractions of each sample and reported the result in terms of dissolution efficacy as a function of the mean radius of the particles of each fraction. A D_R value of 2.96 was for the commercial samples, while 2.76 was for the crystallized particles. According to Equation (29), one can calculate the D_R value in two cases.

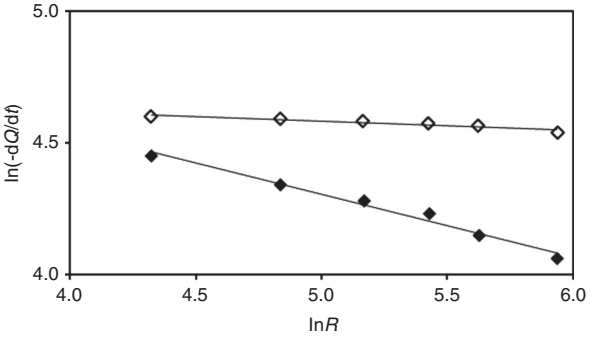

Figure 8 Plot of ln($-dQ/dt$) as a function of ln(R): ◇, commercial samples with D_R=2.96; ◆, crystallized samples with D_R=2.76 (Fini et al. 1996).

On the one hand, R is the particle mean diameter for narrowly sieved fractions, and this case leads to the study of the kinetic order relating to Equation (30) (Tromelin et al. 1996). A set of D_R values could be obtained as a function of time due to the variation of the dissolution rate along with the elapsed time. On the other hand, R could be the size of the particles of each granulometric fraction at different steps of dissolution. Since R is changing along with reaction rate during the dissolving process, it is necessary to fix the kinetic parameter. Tromelin et al. (1996, 2001) selected the experimentally highest value of the dissolution rate for each granulometric fraction and calculated the D_R value from the slope of a logarithm fitting of the highest dissolution rate value and particle radius. The result of Equation (29) reflects the common dissolution behavior of different particles, showing that the dissolution rate is not greatly affected by the size of the particles (Tromelin et al. 1996).

For each granulometric fraction, D_R could be calculated with Equation (30) from the slope of ln(dissolution rate) versus ln(undissolved product level), involving the study of the kinetic order of dissolution and requiring differential dissolution data. Tromelin et al. (1996) found that the reactive fractal dimension did not remain constant due to the discontinuity of the slope along the dissolution, as shown in Figure 9, and the segments of the Richardson plot of the various fractions corresponding to the period when nearly half of product was dissolved were almost parallel. The D_R value obtained ranged from 2.09 to 2.63. However, Bao and Nguyen (2010) directly employed Equation (30) to evaluate the D_R values of gibbsite and diaspore dissolving in NaOH solution under various conditions by carrying out the nonlinear regression analysis. There was only a single D_R value to describe a specific dissolution condition. In addition, the value reflected the capability of a certain condition in extracting aluminum

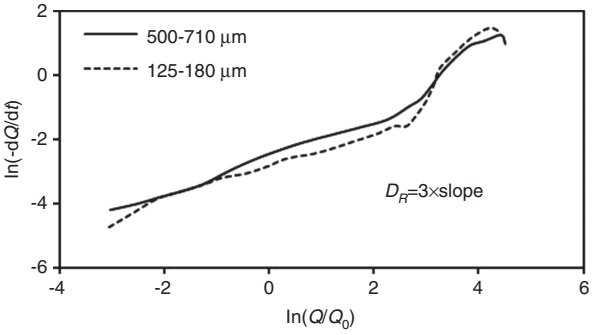

Figure 9 Richardson plot of dissolution profile of different fractions (Tromelin et al. 1996).

from gibbsite/diaspore; the higher dissolution temperature is, the higher is the D_R value.

The D_R values provided by Equations (29) and (30) are different or even contradictory when comparing it with the surface fractal dimension. Since the value of the reactive fractal dimension is necessary to attribute a dissolution mechanism, Tromelin et al. (2001) pointed out that only one way of determination provided some limited information on the dissolution mechanism, which will be discussed in the next section, and the D_R values from the two ways can provide a good prediction of the mechanism.

There are two extreme cases existing in Equation (30). The first case was developed for dissolution under the "far from saturation" conditions, where Q_e-Q_0+$Q \cong Q_e$. Equation (30) transforms into

$$-dQ/dt = kQ_eQ^{D_R/3}. \quad (31)$$

In contrast, when the initial weight in solution is quite high, Q_0 is approximate to the amount of saturate in solution; thus, Equation (30) is reduced to

$$-dQ/dt = kQ^{(D_R+3)/3}. \quad (32)$$

The Hixon-Crowell cube root law equation, the integrated form of Noyes-Whitney equation, was similarly modified from the integration of Equations (31) and (32), which are shown as below, respectively.

$$\left(\frac{3}{D_R\text{-}3}\right)(Q^{(3\text{-}D_R)/3}\text{-}Q_0^{(3\text{-}D_R)/3}) = Q_e kt \quad (33)$$

$$\frac{3}{D_R}(Q^{-D_R/3}\text{-}Q_0^{-D_R/3}) = kt. \quad (34)$$

The simulation study of Equations (33) and (34) performed by Valsami and Macheras (1995) was to generate various D_R values between 1.7 and 3, while the values of Q_0 and Q_e were set as 100 and 1000, respectively. The values of time t were assigned as 0–10 in the case of Equation (33) and 0–100 in the case of Equation (34), which describes the dissolution process when carried out under conditions that are allowed to develop up to saturation. In both cases, the calculated and theoretical D_R values were found to be identical.

Momonaga et al. (1996) suggested that the reactive fractal dimension varies with dissolution behavior and carried the information about the mechanism of the dissolution process. The first group of particles were Smoluchowskian particles, the volume of which was composed of several organized agglomerated growth units. Thus, the molecules of solvent can attack not only their external surfaces but also can penetrate into the inner structure to dissolve the necks of the agglomerated growth units. The value of the reactive fractal dimension of Smoluchowskian particles was characterized as $0.0 \le D_R \le 1.0$. The particles ranging from 30 nm to 5 μm were named Brownian particles, because the solubility of these particles is usually influenced by Brownian motion in the enhanced reactivity; the smaller the size of the particles is, the more vigorous is the Brownian motion of the particles and the more pronounced is the dissolution of particles. The dissolution fractal dimensions of Brownian particles had their typical values as $1.0 \le D_R \le 2.0$. In the case of non-Brownian particles in the size range from 10 μm to 5 mm, the relative slip velocities between the particle and surroundings increase with the size of the objects in an agitated system while Brownian motion is suppressed or even excluded for such big particles. The value of the reactive fractal dimension of this type of particles was between 2.0 and 3.0.

4.3 Interpretation of dissolution mechanism

Table 4 displays both the reactive and surface fractal dimensions following with reaction situations and the application of equation to obtain the dimensions, showing obviously that the value of reactive fractal dimension D_R might be close to D_S or higher or lower than the D_S value. Farin and Avnir (1987) concluded four effects governing the relation between these two dimensions in order:

1. Screening: Some parts of the surface are hindered inside of particle body, and the reactive molecules consequently cannot get access to the inner parts by diffusion. In this case, the reactive fractal dimension D_R is less than D_S.
2. Chemical selectivity: Since the activation energies for the reaction could not distribute homogeneously on

Table 4 Fractal analysis of dissolution.

Material	Reaction	Particle size range, μm (no. of fractions)	Reactive fractal dimension D_R		Surface fractal dimension D_S		References
			Value	Application of formula	Value	Application of formula	
Upper Columbus dolomite ($CaCO_3$-$MgCO_3$)	Acidic dissolution in NH_4Cl	163–2605 (5)	2.15±0.10	Equation (29)	2.91±0.02	Equation (14)	Love and Whittaker 1954, Farin and Avnir 1987, Avnir 1989
Upper Columbus dolomite ($CaCO_3$-$MgCO_3$)	Acidic dissolution in oxalate buffer	163–2605 (5)	2.34±0.04	Equation (29)	2.91±0.02	Equation (14)	Love and Whittaker 1954, Farin and Avnir 1987
Niagara dolomite ($CaCO_3$-$MgCO_3$)	Acidic dissolution in NH_4Cl	163–2605 (5)	2.07±0.06	Equation (29)	2.58±0.01	Equation (14)	Love and Whittaker 1954, Farin and Avnir 1987, Avnir 1989
Niagara dolomite ($CaCO_3$-$MgCO_3$)	Acidic dissolution in oxalate buffer	163–2605 (5)	2.19±0.05	Equation (29)	2.58±0.01	Equation (14)	Love and Whittaker 1954, Farin and Avnir 1987
Niagara dolomite ($CaCO_3$-$MgCO_3$)	Acidic dissolution in NH_4Cl during the first 10% decomposition	81–325 (3)	2.4±0.08	Equation (29)	2.58±0.01	Equation (14)	Love and Whittaker 1954, Farin and Avnir 1987
Niagara dolomite ($CaCO_3$-$MgCO_3$)	Acidic dissolution in NH_4Cl during the first 20% decomposition	81–325 (3)	2.32±0.08	Equation (29)	2.58±0.01	Equation (14)	Love and Whittaker 1954, Farin and Avnir 1987
Niagara dolomite ($CaCO_3$-$MgCO_3$)	Acidic dissolution in NH_4Cl during the first 30% decomposition	81–325 (3)	2.37±0.06	Equation (29)	2.58±0.01	Equation (14)	Love and Whittaker 1954, Farin and Avnir 1987
Niagara dolomite ($CaCO_3$-$MgCO_3$)	Acidic dissolution in NH_4Cl during the first 50% decomposition	81–325 (3)	2.40±0.04	Equation (29)	2.58±0.01	Equation (14)	Love and Whittaker 1954, Farin and Avnir 1987
Niagara dolomite ($CaCO_3$-$MgCO_3$)	Acidic dissolution in NH_4Cl during the first 80% decomposition	81–325 (3)	2.37±0.08	Equation (29)	2.58±0.01	Equation (14)	Love and Whittaker 1954, Farin and Avnir 1987
Nonporous rhombic calcite ($CaCO_3$)	Acidic dissolution in seawater	5, 81	1.96	Equation (29)	2.03	Equation (14)	Walter 1984, Farin and Avnir 1987
Halimeda skeletal carbonate (green algae)	Acidic dissolution in seawater	81–513 (5)	2.05±0.08	Equation (29)	3.02±0.07	Equation (14)	Walter 1984, Farin and Avnir 1987, Avnir 1989
Fungia skeletal carbonate $CaCO_3$	Acidic dissolution in seawater	51–513 (5)	1.98±0.07	Equation (29)	2.73±0.05	Equation (14)	Walter 1984, Farin and Avnir 1987
Clypeaster, skeletal carbonate ($CaCO_3$-$MgCO_3$)	Acidic dissolution in seawater	81–513 (5)	2.15±0.07	Equation (29)	2.69±0.04	Equation (14)	Walter 1984, Farin and Avnir 1987
Hybla alkali feldspar (potassium aluminosilicate)	Dissolution in HCl (pH 3)	56–400 (4)	3.0±0.1	Equation (29)	2.36±0.02 2.09±0.03[a]	Equation (14)	Holdren and Speyer 1985, Farin and Avnir 1987
Hybla alkali feldspar (potassium aluminosilicate)	Dissolution in HCl (pH 5)	56–400 (4)	2.95±0.16	Equation (29)	2.36±0.02	Equation (14)	Holdren and Speyer 1985, Farin and Avnir 1987, Avnir 1989
Hybla alkali feldspar (potassium aluminosilicate)	Dissolution in boric acid buffer (pH 9)	56–400 (4)	3.06±0.06	Equation (29)	2.36±0.02	Equation (14)	Holdren and Speyer 1985, Farin and Avnir 1987
Amelia Courthouse albite (sodium aluminosilicate)	Dissolution in K-biphthalate, KOH buffer (pH 6)	56–400 (4)	2.81±0.01	Equation (29)	2.5–2.6	Equation (14)	Holdren and Speyer 1985, Farin and Avnir 1987
Quartz	Dissolution in HF (3.66 M)	45–1000 (10)	2.14±0.06	Equation (29)	2.1–2.15	Equation (14)	Farin and Avnir 1987
Ottawa sand (quartz)	Dissolution in HF (3.66 M)	89–711 (7)	2.15±0.06	Equation (29)	2.0–2.15	Equation (14)	Farin and Avnir 1987

(**Table 4** Continued)

Material	Reaction	Particle size range, μm (no. of fractions)	Reactive fractal dimension D_R		Surface fractal dimension D_S		References
			Value	Application of formula	Value	Application of formula	
Madagascar quartz	Dissolution in HF (0.1 M)	0.4–16 (14)	1.59±0.05	Equation (29)	1.99±0.06	Equation (14)	Farin and Avnir 1987, Avnir 1989
Madagascar quartz	Dissolution in dilute NaOH	0.4–6 (4)	1.78±0.07	Equation (29)	1.99±0.06	Equation (14)	Farin and Avnir 1987
Tridymite (SiO_2/Na_2SO_4 glass)	Dissolution in HF (0.1 M)	0.4–5.2 (8)	1.77±0.06	Equation (29)	1.82±0.07	Equation (14)	Farin and Avnir 1987
Vitreous silica	Dissolution in HF (0.1 M)	0.4–12.6 (6)	1.95±0.04	Equation (29)	2.03±0.04	Equation (14)	Farin and Avnir 1987
Iceland spar calcite ($CaCO_3$)	Dissolution in HCl (pH 3)	137–631 (5)	1.80±0.06	Equation (29)	2.16±0.04	Equation (14)	Farin and Avnir 1987
Sulfisomezole	Dissolution in distilled water	194–650 (6)	1.89±0.04	Equation (29)			Farin and Avnir 1987
Sulfisomezole	Dissolution in 0.1 and 1% sodium lauryl sulfate	97–650 (7, 9)	2.0	Equation (29)			Farin and Avnir 1987
Sulfamethizole	Dissolution in distilled water	81–650 (7)	2.07±0.04	Equation (29)			Farin and Avnir 1987
Sulfamethizole	Dissolution in 0.1 and 1% sodium lauryl sulfate	97–650 (7, 9)	2.0	Equation (29)			Farin and Avnir 1987
Diclofenac hydroxyethylpyrrolidine	Dissolution in pure water for 10, 20, 30, 40, and 120 min	75–300 (6)	2.74–2.76[b]	Equation (29)	2.14	Equation (10)	Fernández-Hervás et al. 1994
Diclofenac/N-(2-hydroxyethyl) pyrrolidine 1 (DHEP 1)	Dissolution in pure water	50–350 (5)	2.76–2.92[a]	Equation (29)	2.14–2.10[a]	Equation (10)	Fernández-Hervás et al. 1996a
Diclofenac/N-(2-hydroxyethyl) pyrrolidine 2 (DHEP 2)	Dissolution in pure water	50–350 (5)	2.80–2.89[a]	Equation (29)	2.04–2.07[a]	Equation (10)	Fernández-Hervás et al. 1996a
Diclofenac/N-(2-hydroxyethyl) pyrrolidine 3 (DHEP 3)	Dissolution in pure water	50–350 (5)	2.68–2.86[a]	Equation (29)	2.09–2.08[a]	Equation (10)	Fernández-Hervás et al. 1996a
Diclofenac/N-(2-hydroxyethyl) pyrrolidine 4 (DHEP 4)	Dissolution in pure water	50–350 (5)	2.77–2.92[a]	Equation (29)	2.05–2.13[a]	Equation (10)	Fernández-Hervás et al. 1996a
Diclofenac/N-(2-hydroxyethyl) pyrrolidine 5 (DHEP 5)	Dissolution in pure water	50–350 (5)	2.65–2.99[a]	Equation (29)	2.10–2.05[a]	Equation (10)	Fernández-Hervás et al. 1996a
Inert matrix system generated from polymer and drug ClNa (20 wt%)	Dissolution in pure water	50–300 (5)	3.00–3.16[b]	Equation (29)	2.50–2.36[b]	Others	Fernández-Hervás et al. 1996b
Inert matrix system generated from polymer and drug ClNa (50 wt%)	Dissolution in pure water	50–300 (5)	3.02–3.24[b]	Equation (29)	2.50–2.36[b]	Others	Fernández-Hervás et al. 1996b
Inert matrix system generated from polymer and drug ClNa (80 wt%)	Dissolution in pure water	50–300 (5)	3.05–3.51[b]	Equation (29)	2.50–2.36	Others	Fernández-Hervás et al. 1996b
Ursodeoxycholic acid-Li	Dissolution in bidistilled water	50–350 (6)	2.85±0.02	Equation (29)	2.29±0.02	Equation (10)	Fini et al. 1998
Ursodeoxycholic acid-Na	Dissolution in bidistilled water	50–350 (6)	2.84±0.01	Equation (29)	2.15±0.02	Equation (10)	Fini et al. 1998
Ursodeoxycholic acid- K	Dissolution in bidistilled water	50–350 (6)	2.82±0.03	Equation (29)	2.06±0.04	Equation (10)	Fini et al. 1998
Ursodeoxycholic acid-PE	Dissolution in bidistilled water	50–350 (6)	2.79±0.05	Equation (29)	2.43±0.02	Equation (10)	Fini et al. 1998
Ursodeoxycholic acid-Arg	Dissolution in bidistilled water	50–350 (6)	2.79±0.05	Equation (29)	2.02±0.02	Equation (10)	Fini et al. 1998
Ursodeoxycholic acid-Tris	Dissolution in bidistilled water	50–350 (6)	2.50±0.01	Equation (29)	2.09±0.02	Equation (10)	Fini et al. 1998

(**Table 4** Continued)

Material	Reaction	Particle size range, μm (no. of fractions)	Reactive fractal dimension D_R		Surface fractal dimension D_S		References
			Value	Application of formula	Value	Application of formula	
Saccharin	Dissolution in pure water with 0.01% lauryl sulfate sodium	63–250 (4)	2.28	Equation (29)	2.30	Equation (14)	Tromelin et al. 2001
Saccharin	Dissolution in pure water with 0.01% lauryl sulfate sodium	63–100 (1)	2.99–3.79[b]	Equation (30)	2.30	Equation (14)	Tromelin et al. 2001
Saccharin	Dissolution in pure water with 0.01% lauryl sulfate sodium	100–150 (1)	2.68–2.88[b]	Equation (30)	2.30	Equation (14)	Tromelin et al. 2001
Saccharin	Dissolution in pure water with 0.01% lauryl sulfate sodium	150–200 (1)	22.55–3.05[b]	Equation (30)	2.30	Equation (14)	Tromelin et al. 2001
Saccharin	Dissolution in pure water with 0.01% lauryl sulfate sodium	200–250 (1)	2.89–2.96[b]	Equation (30)	2.30	Equation (14)	Tromelin et al. 2001
Commercial sodium cholate	Dissolution in pure water	50–400 (6)	2.96, 2.80–2.83[b]	Equation (29)	2.70–2.96	Equation (10)	Fini et al. 1996
Crystallized sodium cholate	Dissolution in pure water	50–400 (6)	2.76	Equation (29)	2.14	Equation (10)	Fini et al. 1996
Orthoboric acid	Dissolution in bidistilled water	90–500 (5)	2.84, 2.82–2.83[b]	Equation (29)	2.42	Equation (14)	Tromelin et al. 1996
Orthoboric acid	Dissolution in bidistilled water	90–125 (1)	2.09–2.63[b]	Equation (30)	2.02–2.04	Equation (10)	Tromelin et al. 1996
Sulfadiazine	Dissolution in distilled water	74–88 (1)	2.09	Equation (34)	~2.0		Kaneniwa and Watari 1974, Valsami and Macheras 1995
Sulfadiazine	Dissolution in distilled water	125–125 (1)	1.97	Equation (34)	~2.0		Kaneniwa and Watari 1974, Valsami and Macheras 1995
Sulfadiazine	Dissolution in distilled water	149–177 (1)	1.90	Equation (34)	~2.0		Kaneniwa and Watari 1974, Valsami and Macheras 1995
Oxalic acid dehydrate crystals	Dissolution in 0.1 M HCl solution	590–841 (1)	3.0	Equation (33)			Carstensen and Patel 1975, Valsami and Macheras 1995
Gibbsite ($Al(OH)_3$)	Dissolution in 1.2 M NaOH solution at 60°C	45–150 (1)	1.018	Equation (30)			Pereira et al. 2009, Bao and Nguyen 2010
Gibbsite ($Al(OH)_3$)	Dissolution in 1.2 M NaOH solution at 80°C	45–150 (1)	1.452	Equation (30)			Pereira et al. 2009, Bao and Nguyen 2010
Gibbsite ($Al(OH)_3$)	Dissolution in 1.2 M NaOH solution at 100°C	45–150 (1)	2.928	Equation (30)			Pereira et al. 2009, Bao and Nguyen 2010
Diaspore (AlOOH)	Dissolution in 4 M NaOH solution at 240°C	0.3–630 (1)	2.3122	Equation (30)			Bao 2011, Bao et al. 2013
Diaspore (AlOOH)	Dissolution in 6 M NaOH solution at 240°C	0.3–630 (1)	2.5747	Equation (30)			Bao 2011, Bao et al. 2013

[a]Fractal dimension after dissolution.
[b]Fractal dimension as a function of dissolution time.

the surface in many cases, and the reactive sites are subsets of all surface sites, it is easy to expect $D_R<D_S$ when this effect operates.

3. Roughening and smoothing: In the case of the reaction, the morphology of a particle surface may change. If this change takes place at the very beginning of the reaction, D_R may be larger (roughening) or smaller (smoothing) than D_R.
4. Trapping and reaction in pore volumes: Reactive molecules may be trapped in a small proportion of cracks and pores where it is difficult to be released either because of diffusional limitation or because of stronger adsorbate-adsorbent interactions. Unlike the screening effect, a trapped molecule will have sufficient time to probe the surface irregularity of these traps. If the surface of the trap is rougher than the rest of the surface, one might expect a $D_R>D_S$ situation.

The results of Equation (30) are usually in a value range, as a function of dissolving time, describing the dissolving situation at predetermined time periods. The large value range can be explained as a consequence of the competition between the two phenomena of roughening and smoothing (Tromelin et al. 1996). On the contrary, the D_R values obtained at various dissolving times remain almost the same, because the reactive surface morphology remains constant either at the beginning or ending of the dissolution process and the reactive surface offered to the dissolution medium changes in magnitude instead of morphology (Fernández-Hervás et al. 1994). If D_R yields quickly to constant values, it indicates a slow dissolving process (Fernández-Hervás et al. 1996b). During the dissolution process of the matrix system, the low value of D_R is indicative of low reactivity, and only the particles connected to the surface are being dissolved. In contrast, an elevated D_R value suggests that a great amount of reactive surface exposes to dissolution medium, and the dissolution process is very fast (Fernández-Hervás et al. 1996b).

The D_R and D_S values are practically equal. $D_R\approx D_S$, indicates that there are no privileged sites of reactivity on the surface of the dissolving particle or that all the points constituting the particle surface participate to the same extent in the dissolution. In the case of the particles being formed by very irregular agglomerates, although the surface available to the dissolution medium is expected to be larger than that of a single and isolated particle, the surface irregularities are uniformly distributed on the particles, as documented by the high value; also, the dissolution process is uniform on the whole surface (Fini et al. 1996). The relation can also reflect that the reaction occurs at the whole surface where the main responsible factors are both the roughening and/or trapping of the dissolution medium in micropores ($D_R>D_S$) and the diffusional inaccessibility of parts of surface or chemical selectivity due to heterogeneously distribution of activation energy ($D_R<D_S$) (Tromelin et al. 2001).

In the case of $D_R>D_S$, it can be suggested that, as one hypothesis, the reaction occurs selectively at the cracks of the surface and continues by roughening at these sites; then, the dissolution medium is trapped in these formed micropores or holes (Tromelin et al. 2001). Another hypothesis (Fernández-Hervás et al. 1996b) is that the two phenomena of both roughing and trapping effects govern the dissolution process simultaneously, and the trapping of the dissolution medium in pores takes place along the process. Corresponding to the particles with smooth surface, there is still a situation of $D_R>D_S$ due to the fact that the particles are constituted by an agglomeration of cubes. The boundary particles that are composed by fissures and cracks cannot be measured by the Richardson method. Thus, the "real" surface exposing to the dissolution medium is more irregular than that offered by a single particle (Fernández-Hervás et al. 1994, 1996a).

The weak dependence between the particle diameters and the reactive surface area suggests that this phenomenon can be attributed to a very high degree of porosity. However, important roughening phenomena occur only on some sites but not on all the bulk surface of the particles. In this context, the dissolution can occur in the pore volumes where the surface is rougher than on the rest of the particle surface. On the contrary, water molecules can be trapped at the reactive sites heterogeneously distributed on the surface. In this case, the number of reactive sites should be very similar regardless of the particle size, and the size effect induces a weak dependence on the specific population of active sites (Tromelin et al. 1996).

There is also another case that the samples with the same compounds have similar D_R values but quite different surface fractal dimensions, which is suggested by the nature of the dissolving compounds instead of the nature of the surface. Because the diffusion layer surrounding a dissolving particle is regarded to have a solute concentration near its saturation value, the rate of movement of the solute toward the surface of particles is governed by the diffusion of the monomer and self-aggregates in solution across the stagnant diffusion layer. If the solute is a kind of anionic surfactant that can decrease the solid/liquid interfacial tension and improve the wettability of the particles, the dissolution efficacy consequently increases. Meanwhile, the aggregation number of the sample micelles is

so low that the difference between monomers and aggregates can be neglected. Under these conditions, the difference in the surface irregularity found for the samples could be cancelled; therefore, the reactive dimension to dissolution is less dependent on the particle surface (Fini et al. 1996, 1998). The D_R value is usually higher than the corresponding surface fractal dimension, D_R value (Fini et al. 1996, 1998).

5 Conclusion and future challenge

In the practical dissolving process, the morphology of a bulk of particles is irregular and changes while the reaction proceeds. In terms of an individual particle, the surface structure and particle size are altered due to the erosion of the solute; the variation of the PSD occurs as a whole. Consequently, the reaction rate will vary with the elapsed time. The fractal theory is used to interpret the popular and chaos system using an indicator, fractal dimension, to describe the degree of irregularity. A variety of fractal analysis strategies for fractal surface, PSD, and reaction have been developed to calculate the corresponding fractal dimension over the past few decades. The surface fractal dimension could be estimated from the boundary fractal dimension and adsorption method, including the monolayer adsorption based on both adsorbate and adsorbent and the multilayer adsorption based on a single isotherm curve. However, for the same object, the surface fractal dimension obtained varies with the method, since no method is universal due to its limitations. The irregular degree of the PSD could be implied by the distribution fractal dimension, which is calculated by a single fractal model in the case of the object with uniform texture and by the piecewise fractal model when the particles contain two or more textures. Similar with the surface area, the reactive surface area is indicated by the reaction dimension, which depends on the reaction and/or dissolution of the process. Two formulations relating to the reaction rate were extensively used to evaluate the reactive fractal dimension, the comparison of which with the surface fractal dimension can explore the dissolution mechanism to some extent.

In spite of the various approaches to the analysis of fractal particles, the authors found that there are still great challenges existing in the research of dissolution fractals compared to the published results. In practice, especially at the industrial scale, the dissolution process involves solids consisting of a wide range or distribution of particle size and performs the particle shrinkage process. This fact has been confirmed by the research of dissolving chemical reagent (Sun et al. 2009), minerals (Haenchen et al. 2007), and drugs. In this case, the concept of average size in Equations (14) and (29) for surface and reactive fractal dimension, respectively, might bring in the questionable results. Although the problem has been avoided as much as possible by using the particle fractions with a narrow size range, it must be noted that both the particle size and size range alter with dissolution proceeding. To some extent, the fractal dimension values of the undissolved particles obtained from the equations might be dependable, but one will doubt the result indicating the irregularity while or after dissolving. The PSD was combined with the shrinking core model by Gbor and Jia (2004) and LeBlanc and Fogler (1987), who proposed the population balance model and particle growth (decrease) rate during dissolution, which were then considered as an important influence factor on the dissolving kinetics in the latter research (Giona et al. 2002, Haenchen et al. 2007) but without fractal theory. Therefore, we recommend that the PSD should be performed on the surface and reactive fractal models.

On the contrary, the primary implication of the fractal dimension of the PSD is the texture of a population of particles. Most of the published research focused on the soils in a specified area, with respect to the texture distribution, but seldom on the dissolution process. The authors suggest that, for mineral dissolution, the PSD fractal dimension that changes with dissolution proceeding could reflect the transformation of textures as a result of the reaction with solute. Since a mineral is an element or chemical compound that is normally crystalline and has been formed as a result of a geological processes, the ground mineral particle has an asymmetrical distribution of the compositions both on the particle surface and in the body. The elements selectively dissolve into the solution. This is the reason that the surface structure changes during dissolving. If the cracks are deep enough through the particle body, one particle will break into two or even more partitions. Breakage takes place along with time. In this situation, the more insoluble elements (originates from both the mineral and the product) a particle contains, the larger is the particle size. How the particle size distributes is capable of indexing the change in the texture of the mineral during dissolution process.

As discussed before, the reactive fractal dimension from Equation (29) is a function of dissolving time, and Equation (30) gives a set of values indicating several segments of the dissolution process when applying the

common method of logarithm due to the changing slope of ln(dissolution rate) versus ln(undissolved product). However, the dissolution process is a whole system that could be treated as an object like a curve or a fractal particle. It is reasonable and desired to use a single fractal value to express the degree of chaos of the process. Although Bao and Nguyen (2010) achieved their model, which only described the dissolution process in an infinite time range, it might not be available in the case when the process is controlled at a limited period or is half-dissolved. It is recommended that new models should be developed to estimate one value of the reactive dimension for the whole process under an arbitrarily temporal controlling condition.

According to the published literature, the mechanism of dissolution was explored by comparing the values between the surface fractal dimension and the reaction fractal dimension. The case is that a group of particles could see the various values of the surface fractal dimension by applying different methods. In general, some methods can provide the relatively higher values than others, originating from the limitation of the methods. The interpretation of the mechanism when $D_R > D_s$ is definitely different, even contrast, with that in the case of $D_R < D_s$. We suggest that it is necessary to fix the criteria that indicate the properties of the suitable object for each method of surface fractal determination.

With the development of material manufacturing, the nanoparticles have become a subject of great importance in the use of advanced materials. It is necessary to investigate the dissolving process of the nanoparticles to get an insight of its behavior. The approaches to the analysis of fractal particles reviewed in this paper are useful for the scholar's further investigation but not yet enough. The reason is that the fractal analysis methods in this paper are almost based on the experimental data of real particles. In the case of nanoparticles, there are only a few investigations on the dissolution. The reported investigation was for the hypothetical nanoparticles instead for the practical ones (Mihranyan and Strøme 2007). Thus, the data of the dissolving process for setting up a fractal analysis system for nanoparticles are lacking. We consider that a new fractal analysis system needs to be presented by carrying out the practical nanoparticle dissolving experiment and then this will help the investigator to better understand the nanoparticles in return.

Acknowledgments: This paper is financially supported by State Key Lab of Advanced Welding and Joining, Harbin Institute of Technology.

References

Avnir D, editor. The fractal approach to heterogeneous chemistry. Chichester: John Wiley & Sons, 1989.

Avnir D, Farin D, Pfeifer P. Chemistry in noninteger dimensions between two and three. II. Fractal surfaces of adsorbents. J Chem Phys 1983; 79: 3566–3571.

Avnir D, Farin D, Pfeifer P. Molecular fractal surfaces. Nature (London) 1984; 308: 261–263.

Avnir D, Farin D, Pfeifer P. Surface geometric irregularity of particulate materials: the fractal approach. J Colloid Interface Sci 1985; 103: 112–123.

Bao L. Study on thermal analysis kinetics and kinetic model for leaching bauxite. Shenyang: Northeastern University, 2011.

Bao L, Nguyen AV. Developing a physically consistent model for gibbsite leaching kinetics. Hydrometallurgy 2010; 104: 86–98.

Bao L, Zhang T-A, Long WM, Nguyen AV, Lv G, Ma J, Liu Y. Particle size distribution model for kinetics of digesting alumina. Light Metals 2013; 59–64.

Ben Ohoud M, Obrecht F, Gatineua L, Levitz P, Van Damme H. Surface area, mass fractal dimension, and apparent density of powders. J Colloid Interface Sci 1988; 124: 156–161.

Bird NRA, Perrier E, Rieu M. The water retention function for a model of soil structure with pore and solid fractal distributions. Eur J Soil Sci 2000; 51: 55–63.

Birdi KS, editor. Fractals in chemistry, geochemistry, and biophysics. New York: Plenum Press, 1993.

Bittelli M, Campbell GS, Flury M. Characterization of particle-size distribution in soils with a fragmentation model. Soil Sci Soc Am J 1999; 63: 782–788.

Blacher S, Heinrichs B, Sahouli B, Pirard R, Pirard JP. Fractal characterization of wide pore range catalysts: application to Pd-Ag/SiO_2 xerogels. J Colloid Interface Sci 2000; 226: 123–130.

Boldyrev VV, Bulens M, Delmon B, editors. The control of the reactivity of solids. Amsterdam: Elsevier Scientific Publishing Company, 1979.

Brunauer S, Emmett PH, Teller E. Adsorption of gases in multimolecular layers. J Am Chem Soc 1938; 60: 309–319.

Burns H Jr, Carpenter DK. Adsorption of polystyrene on porous and nonporous adsorbents. Macromolecules 1968; 1: 384–389.

Canals M, Meunier JD. A model for porosity reduction in quartzite reservoirs by quartz cementation. Geochim Cosmochim Acta 1995; 59: 699–709.

Carstensen JT, Patel M. Dissolution patterns of polydisperse powders oxalic acid dihydrate. J Pharm Sci 1975; 64: 1770–1776.

Chen H-L, Chang Y-I. Neighbor-finding based on space-filling curves. Inform Syst 2005; 30: 205–226.

Colón CFJ, Oelkers EH, Schott J. Experimental investigation of the effect of dissolution on sandstone permeability, porosity, and reactive surface area. Geochim Cosmochim Acta 2004; 68: 805–817.

Corn M, Stein F, Hammad Y, Manekshaw S, Freedman R, Hartstein AM. Physical and chemical properties of respirable coal dust from two United States mines. Am Ind Hyg Assoc J 1973; 34: 279–285.

Cristea LL, Steinsky B. Connected generalised Sierpinski carpets. Topol Appl 2010; 157: 1157–1162.

Cui L, An L, Gong W. Effects of process parameters on the comminution capability of high pressure water jet mill. Int J Miner Process 2006; 81: 113–121.
Drake JM, Levitz P, Sinha S. General scaling phenomena in porous silica gels as probed by SAXS and molecular adsorption (tiling). Mater Res Soc Symp Proc 1986; 73: 305–319.
El Shafei GMS, Philip CA, Moussa NA. Fractal analysis of hydroxyapatite from nitrogen isotherms. J Colloid Interface Sci 2004; 277: 410–416.
Emmanuel S, Berkowitz B. Mixing-induced precipitation and porosity evolution in porous media. Adv Water Resour 2005; 28: 337–344.
Ersahin S, Gunal H, Kutlu T, Yetgin B, Coban S. Estimating specific surface area and cation exchange capacity in soils using fractal dimension of particle-size distribution. Geoderma 2006; 136: 588–597.
Esquena J, Solans C, Llorens J. Nitrogen sorption studies of silica particles obtained in emulsion and microemulsion media. J Colloid Interface Sci 2000; 225: 291–298.
Falconer K, editor. Fractal geometry mathematical foundations and applications. Chichester: John Wiley & Sons, 1990.
Farin D, Avnir D. Reactive fractal surface. Phys Chem 1987; 91: 5517–5521.
Farin D, Avnir D. The reaction dimension in catalysis on dispersed metals. J Am Chem Soc 1988; 110: 2039–2045.
Farin D, Avnir D. Use of fractal geometry to determine effects of surface morphology on drug dissolution. J Pharm Sci 1992; 81: 54–57.
Farin D, Volpert A, Avnir D. Determination of adsorption conformation from surface resolution analysis. J Am Chem Soc 1985; 107: 3368–3370.
Fernández-Hervás M-J, Holgado M-A, Rabasco A-M, Fini A. Use of fractal geometry on the characterization of particles morphology: application to the diclofenac hydroxyethylpirrolidine salt. Int J Pharm 1994; 108: 187–194.
Fernández-Hervás MJ, Holgado MA, Rabasco AM, Fazio G, Fini A. Fractal and reactive dimension of a diclofenac salt: effect of the experimental conditions. Int J Pharm 1996a; 136: 101–106.
Fernández-Hervás MJ, Vela MT, Fini A, Rabasco AM. Fractal and reactive dimension in inert matrix systems. Int J Pharm 1996b; 130: 115–119.
Fini A, Fazio G, Fernandez-Hervas MJ, Holgado MA, Rabasco AM. Fractal analysis of sodium cholate particles. J Pharm Sci 1996; 85: 971–975.
Fini A, Fazio G, Holgado MA, Fernàndez-Hervàs MJ. Fractal and reactive dimensions of some ursodeoxycholic acid salts. Int J Pharm 1998; 171: 45–52.
Frank H, Zwanziger H, Welsch T. Fractal surface dimension of silica used in liquid chromatography. Fresenius Z Anal Chem 1987; 326: 153–154.
Fredrich JT, Greaves KH, Martin JW. Pore geometry and transport properties of Fontainebleau sandstone. Int J Rock Mech Mining Sci Geomech Abstr 1993; 30: 691–697.
Friesen WI, Mikula RJ. Fractal dimensions of coal particles. J Colloid Interface Sci 1987; 120: 263–271.
Gasparini FM, Mhlanga S. Fractal surface dimensionality and finite-size scaling at the superfluid transition of confined helium-4. Phys Rev B Condens Matter 1986; 33: 5066–5069.
Gautier J-M, Oelkers EH, Schott J. Are quartz dissolution rates proportional to B.E.T. surface areas? Geochim Cosmochim Acta 2001; 65: 1059–1070.
Gbor PK, Jia CQ. Critical evaluation of coupling particle size distribution with the shrinking core model. Chem Eng Sci 2004; 59: 1979–1987.
Giona M, Adrover A, Pagnanelli F, Toro L. A closed-form solution of population-balance models for the dissolution of polydisperse mixtures. Chem Eng J 2002; 87: 275–284.
Gouze P, Luquot L. X-ray microtomography characterization of porosity, permeability and reactive surface changes during dissolution. J Contam Hydrol 2011; 120–121: 45–55.
Grandstaff DE. Changes in surface area and morphology and the mechanism of forsterite dissolution. Geochim Cosmochim Acta 1978; 42: 1899–1901.
Gurnyk TM, Trypolskyi AI, Ivashchenko TS, Strizhak PE. Porosity and fractality of yttria stabilized zirconia nanopowders obtained by microwave assisted synthesis and calcined at different temperature. J Non-Cryst Solids 2010; 356: 941–944.
Haenchen M, Krevor S, Mazzotti M, Lackner KS. Validation of a population balance model for olivine dissolution. Chem Eng Sci 2007; 62: 6412–6422.
Hailin Z, Bloom PR, Nater EA. Change in surface area and dissolution rates during hornblende dissolution at pH 4.0. Geochim Cosmochim Acta 1993; 57: 1681–1689.
Hodson ME. Does reactive surface area depend on grain size? Results from pH 3, 25°C far-from-equilibrium flow-through dissolution experiments on anorthite and biotite. Geochim Cosmochim Acta 2006; 70: 1655–1667.
Holdren GR, Speyer PM. Reaction rate-surface area relationships during the early stages of weathering – I. Initial observation. Geochim Cosmochim Acta 1985; 49: 675–681.
Hou Q-F, Lu X-C, Liu X-D, Hu B-X, Cui J-Q, Shen J. The surface fractal investigation on carbon nanotubes modified by the adsorption of poly(acrylic acid). Surf Coat Technol 2005; 190: 394–399.
Hua X, editor. Introduction of kinetics in metallurgical process. Beijing: Metallurgical Industry Press, 2004.
Huang PM, Senesi N, Buffle J, editors. Structure and surface reaction of soil particles. Chichester: John Wiley & Sons Ltd., 1998.
Hyslip JP, Vallejo LE. Fractal analysis of the roughness and size distribution of granular materials. Eng Geol 1997; 48: 231–244.
Inoue N, Matsumoto A, Suzuki T, Ozeki S, Kaneko K. Photoadsorption of sulfur dioxide on synthetic goethites. Langmuir 1988; 4: 774–776.
Jaroniec M, Kruk M, Olivier J. Fractal analysis of composite adsorption isotherms obtained by using density functional theory data for argon in slitlike pores. Langmuir 1997; 13: 1031–1035.
Kameyama A. Julia sets and self-similar sets. Topol Appl 1993; 54: 241–251.
Kaneko K, Fukuzaki N, Kakei K, Suzuki T, Ozeki S. Enhancement of nitric oxide dimerization by micropore fields of activated carbon fibers. Langmuir 1989a; 5: 960–965.
Kaneko K, Suzuki T, Kakei K. Phase transition of nitrogen molecules filled in micropores of micrographitic carbons. Langmuir 1989b; 5: 879–881.
Kaneko K, Sato M, Suzuki T, Fujiwara Y, Nishikawa K, Jaroniec M. Surface fractal dimension of microporous carbon fibers by nitrogen adsorption. J Chem Soc Faraday Trans 1991; 87: 179–184.
Kaneniwa N, Watari N. Dissolution of slightly soluble drugs. I. Influence of particle size on dissolution behavior. Chem Pharm Bull 1974; 22: 1699–1705.

Kaye BH. The description of two-dimensional rugged boundaries in fine-particle science by means of fractal dimensions. Powder Technol 1986; 46: 245–254.
Kaye BH, Leblanc JE, Abbot P. Fractal description of the structure of fresh and eroded aluminum shot fineparticles. Particle Charact 1985; 2: 56–61.
Kennedy HC. Peano's concept of number. Historia Mathematica 1974; 1: 387–408.
Lüttge A, Winkler U, Lasaga AC. Interferometric study of the dolomite dissolution: a new conceptual model for mineral dissolution. Geochim Cosmochim Acta 2003; 67: 1099–1116.
Lauwerier H, editor. Fractals. Princeton: Princeton University Press, 1991.
Le Gallo Y, Bildstein O, Brosse E. Coupled reaction-flow modeling of diagenetic changes in reservoir permeability, porosity and mineral compositions. J Hydrol 1998; 209: 366–388.
LeBlanc SE, Fogler HS. Population balance modeling of the dissolution of polydisperse solid: rate limiting regimes. AIChE J 1987; 33: 54–63.
Lee C-K. Fractal surface analysis by using capillary condensation data. Ind Eng Chem Res 1998; 37: 3939–3942.
Lee G-J, Pyun S-I. The effect of pore structures on fractal characteristics of meso/macroporous carbons synthesised using silica template. Carbon 2005; 43: 1804–1808.
Lee C-K, Tsay C-S. Surface fractal dimensions of alumina and aluminum borate from nitrogen isotherms. J Phys Chem B 1998; 102: 4123–4130.
Leeson LJ, Carstensen JT, editors. Dissolution technology. Washington, DC: Whitlock Press, Inc., 1974.
Levenspiel O, editor. Chemical reaction engineering. New York: John Wiley & Sons, 1972.
Li Y, Long C, Tao W, Li A, Zhang Q. Fractal dimensions of macroporous and hypercrosslinked polymeric adsorbents from nitrogen adsorption data. J Chem Eng Data 2010; 55: 3147–3150.
Lichtner PC. The quasi-stationary state approximation to coupled mass transport and fluid-rock interaction in a porous medium. Geochim Cosmochim Acta 1988; 52: 143–165.
Liu X. Four alternative patterns of the Hilbert curve. Appl Math Comput 2004; 147: 741–752.
Liu X, Zhang G, Heathman GC, Wang Y, Huang C-h. Fractal features of soil particle-size distribution as affected by plant communities in the forested region of Mountain Yimeng, China. Geoderma 2009; 154: 123–130.
Liu J, Jiang X, Huang X, Wu S. Morphological characterization of super fine pulverized coal particle. Part 4. Nitrogen adsorption and small angle X-ray scattering study. Energy Fuels 2010; 24: 3072–3085.
Love KS, Whittaker CW. Surface area and reactivity of typical [agricultural] limestones. J Agric Food Chem 1954; 2: 1268–1272.
Lu P, Jefferson IF, Rosenbaum MS, Smalley IJ. Fractal characteristics of loess formation: evidence from laboratory experiments. Eng Geol 2003; 69: 287–293.
Ma J, Qi H, Wong P-Z. Experimental study of multilayer adsorption on fractal surfaces in porous media. Phys Rev E 1999; 59: 2049.
Mahnke M, Mögel HJ. Fractal analysis of physical adsorption on material surfaces. Colloid Surf A 2003; 216: 215–228.
Mandelbrot BB, editor. The fractal geometry of nature. New York: W.H. Freeman and Company, 1983.
Mihranyan A, Strøme M. Solubility of fractal nanoparticles. Surf Sci 2007; 601: 315–319.
Mihranyan A, Muhel M, Stromme M. Influence of fractal surface dimension on the dissolution process of sparingly soluble $CaCO_3$ microparticles. Appl Phys A Mater Sci Process 2009; 94: 299–305.
Millán H, González-Posada M, Aguilar M, Domínguez J, Céspedes L. On the fractal scaling of soil data. Particle-size distributions. Geoderma 2003; 117: 117–128.
Milosevic NT, Ristanovic D. Fractal and nonfractal properties of triadic Koch curve. Chaos Solitons Fractals 2007; 34: 1050–1059.
Momonaga M, Stávek J, Ulrich J. Interpretation of dissolution rates by the reaction fractal dimensions. J Cryst Growth 1996; 166: 1053–1057.
Mortimer M, Taylor P, editors. Chemical kinetics and mechanism. Glasgow: Royal Society of Chemistry, 2002.
Nay MA, Morrison JL. The molecular adsorption areas of hydrocarbon gases on charcoal. Can J Res Sect B 1949; 27B: 205–214.
Neimark AV. Calculating surface fractal dimensions of adsorbents. Adsorpt Sci Technol 1990a; 7: 210–219.
Neimark AV. Determination of surface fractal dimensions from experimental adsorption data. Zh Fiz Khim 1990b; 64: 2593–2605.
Neimark AV. Thermodynamic method for calculating the surface fractal dimensionality. Pis'ma Zh Eksp Teor Fiz 1990c; 51: 535–538.
Neimark AV, Hanson M, Unger KK. Fractal analysis of the distribution of high-viscosity fluids in porous supports. J Phys Chem 1993; 97: 6011–6015.
Noiriel C, Gouze P, Bernard D. Investigation of porosity and permeability effects from microstructure changes during limestone dissolution. Geophys Res Lett 2004; 31: L24603.
Noiriel C, Luquot L, Madé B, Raimbault L, Gouze P, van der Lee J. Changes in reactive surface area during limestone dissolution: an experimental and modelling study. Chem Geol 2009; 265: 160–170.
Orkoula MG, Koutsoukos PG. Dissolution effects on specific surface area, particle size, and porosity of pentelic marble. J Colloid Interface Sci 2001; 239: 483–488.
Paramanathan P, Uthayakumar R. Fractal interpolation on the Koch curve. Comput Math Appl 2010; 59: 3229–3233.
Peitgen H-O, Jurgens H, Saupe D, editors. Chaos and fractals. New York: Springer, 2004.
Peng J, Wang S. Correlation between microstructure and performance of Pt/TiO_2 catalysts for formaldehyde catalytic oxidation at ambient temperature: effects of hydrogen pretreatment. J Phys Chem 2007; 111: 9897–9904.
Penrose R, editor. The road to reality: a complete guide to the laws of the universe. New York: A.A. Knopf, 2005.
Pereira JAM, Schwaab M, Dell'Oro E, Pinto JC, Monteiro JLF, Henriques CA. The kinetics of gibbsite dissolution in NaOH. Hydrometallurgy 2009; 96: 6–13.
Pierre L, editor. Preparative chemistry using supported reagents. London: Academic Press, 1987.
Pfeifer P, Avnir D. Chemistry in noninteger dimensions between two and three. I. Fractal theory of heterogeneous surfaces. J Chem Phys 1983; 79: 3558–3565.

Pfeifer P, Cole MW. Fractals in surface science: scattering and thermodynamics of adsorbed films. II. N J Chem 1990; 14: 221–232.
Pfeifer P, Obert M, Cole MW. Fractal BET and FHH theories of adsorption: a comparative study. Proc R Soc London A 1989a; 423: 169–188.
Pfeifer P, Wu YJ, Cole MW, Krim J. Multilayer adsorption on a fractally rough surface. Phys Rev Lett 1989b; 62: 1997.
Prosperini N, Perugini D. Particle size distributions of some soils from the Umbria Region (Italy): fractal analysis and numerical modelling. Geoderma 2008; 145: 185–195.
Prouzet E, Boissière C, Kim SS, Pinnavaia TJ. Roughness of mesoporous silica surfaces deduced from adsorption measurements. Micropor Mesopor Mater 2009; 119: 9–17.
Reddy MM, Claassen HC. Specific surface area of a crushed welded tuff before and after aqueous dissolution. Appl Geochem 1994; 9: 223–233.
Rizkalla N, Hildgen P, Thibert R. Influence of the fractal character of model substances on their reactivity at solid-liquid interfaces. J Colloid Interface Sci 1999; 215: 43–53.
Rozic LS, Petrovic SP, Novakovic TB, Cupic ZD, Grbavcic ZB, Jovanovic DM. Textural and fractal properties of CuO/Al_2O_3 catalyst supports. Chem Eng J 2006; 120: 55–61.
Rozic L, Novakovic T, Petrovic S, Vukovic Z, Cupic Z. Fractal analysis of physical adsorption on surfaces of acid activated bentonites from Serbia. Chem Ind Chem Eng Q 2008; 14: 227–229.
Sahouli B, Blacher S, Brouers F. Applicability of the fractal FHH equation. Langmuir 1997; 13: 4391–4394.
Sahouli B, Blacher S, Brouers F, Chahed L. Fractal analysis methods to characterize porous solids using nitrogen adsorption data. Can J Phys 1999; 77: 653–658.
Scott WT, Wheatcraft SW. Fractal scaling of soil particle-size distributions: analysis and limitations. Soil Sci Soc Am J 1992; 56: 362–369.
Shih J-Y, Chang T-P, Hsiao T-C. Effect of nanosilica on characterization of Portland cement composite. Mater Sci Eng A 2006; 424: 266–274.
Shiraki R, Rock PA, Casey WH. Dissolution kinetics of calcite in 0.1M NaCl solution at room temperature: an atomic force microscopic (AFM) study. Aquat Geochem 2000; 6: 87–108.
Smith MA, Lobo RF. A fractal description of pore structure in block-copolymer templated mesoporous silicates. Micropor Mesopor Mater 2010; 131: 204–209.
Sprecher DA, Draghici S. Space-filling curves and Kolmogorov superposition-based neural networks. Neural Netw 2002; 15: 57–67.
Stós A. Boundary Harnack principle for fractional powers of Laplacian on the Sierpinski carpet. Bull Sci Math 2006; 130: 580–594.
Su YZ, Zhao HL, Zhao WZ, Zhang TH. Fractal features of soil particle size distribution and the implication for indicating desertification. Geoderma 2004; 122: 43–49.
Sun Y, Song X, Wang J, Luo Y, Yu J. On-line monitoring of lithium carbonate dissolution. Cryst Res Technol 2009; 44: 1223–1229.
Tasdemir A. Fractal evaluation of particle size distributions of chromites in different comminution environments. Miner Eng 2009; 22: 156–167.
Thibert R, Akbarieh M, Tawashi R. Application of fractal dimension to the study of the surface ruggedness of granular solids and excipients. J Pharm Sci 1988; 77: 724–726.
Tromelin A, Gnanou J-C, Andres C, Pourcelot Y, Chaillot B. Study of morphology of reactive dissolution interface using fractal geometry. J Pharm Sci 1996; 85: 924–928.
Tromelin A, Hautbout G, Pourcelot Y. Application of fractal geometry to dissolution kinetic study of a sweetener excipient. Int J Pharm 2001; 224: 131–140.
Turcotte DL. Fractals and fragmentation. J Geophys Res 1986; 91: 1921–1926.
Urano K, Omori S, Yamamoto E. Prediction method for adsorption capacities of commercial activated carbons in removal of organic vapors. Environ Sci Technol 1982; 16: 10–14.
Valsami G, Macheras P. Determination of fractal reaction dimension in dissolution studies. Eur J Pharm Sci 1995; 3: 163–169.
van den Vlekkert H, Bousse L, de Rooij N. The temperature dependence of the surface potential at the alumina/electrolyte interface. J Colloid Interface Sci 1988; 122: 336–345.
Walter LM. Reactive surface area of skeletal carbonates during dissolution: effect of grain size. J Sediment Petrol 1984; 54: 1081–1090.
Wang F, Li S. Determination of the surface fractal dimension for porous media by capillary condensation. Ind Eng Chem Res 1997; 36: 1598–1602.
Wang X, Li M-H, Liu S, Liu G. Fractal characteristics of soils under different land-use patterns in the arid and semiarid regions of the Tibetan Plateau, China. Geoderma 2006; 134: 56–61.
Wang Y, Du B, Dou X, Liu J, Shi B, Wang D, Tang H. Study on the pore surface fractal dimension and surface acid-base properties of natural particles around Guanting reservoir. Colloid Surf A 2007; 307: 16–27.
Watt-Smith MJ, Edler KJ, Rigby SP. An experimental study of gas adsorption on fractal surfaces. Langmuir 2005; 21: 2281–2292.
Watt-Smith MJ, Rigby SP, Ralph TR, Walsh FC. Characterisation of porous carbon electrode materials used in proton exchange membrane fuel cells via gas adsorption. J Power Source 2008; 184: 29–37.
Wu Q, Borkovec M, Sticher H. On particle-size distributions in soils. Soil Sci Soc Am J 1993; 57: 883–890.
Xu BA, Wingate C, Smith P. The effect of surface area on the modelling of quartz dissolution under conditions relevant to the Bayer process. Hydrometallurgy 2009; 98: 108–115.
Yao Y, Liu D, Tang D, Tang S, Huang W. Fractal characterization of adsorption-pores of coals from North China: an investigation on CH_4 adsorption capacity of coals. Int J Coal Geol 2008; 73: 27–42.

Dr. Li Bao, majoring in nonferrous metallurgy and nonferrous material forming, focuses on the fractals to explore the leaching process of bauxite particles and develops processing kinetic models.

Dr. Jia Ma researches on powder metallurgy and nonferrous material forming.

Weimin Long, professor of nonferrous metal, is interested in the basic research including the kinetics of material forming by carrying out the fractal theory.

Peng He, professor of alloy forming, focuses on the kinetics of the forming process.

Ting-an Zhang, professor of chemical engineering, researches in the fields of hydrometallurgy and particle dissolution.

Anh V. Nguyen is a professor of chemical engineering, whose main research areas are hydrometallurgy, froth flotation, and coal separation.